Doctoral Thesis

Power Control Techniques in Wireless Power Transfer System

Kyungmin Na

Department of Electrical Engineering

Graduate School of UNIST

2018

Power Control Techniques in Wireless Power Transfer System

Kyungmin Na

Department of Electrical Engineering

Graduate School of UNIST

Power Control Techniques in Wireless Power Transfer System

A dissertation
submitted to the Graduate School of UNIST
in partial fulfillment of the
requirements for the degree of
Doctor of Philosophy

Kyungmin Na

12. 11. 2017
Approved by

Advisor
Franklin Bien

Power Control Techniques in Wireless Power Transfer System

Kyungmin Na

This certifies that the thesis/dissertation of Kyungmin Na is approved.

12/11/2017

signature

Advisor: Franklin Bien

signature

Jingook Kim: Thesis Committee Member #1

signature

Katherine A. Kim: Thesis Committee Member #2

signature

Seong-Jin Kim: Thesis Committee Member #3

signature

Ki Jin Han: Thesis Committee Member #4;

Abstract

Wireless power transfer (WPT) technology has attract the attentions of researchers and industrial for new method of power transfer mechanism. WPT technology enables contactless energy transfer between two resonators through a magnetic field. WPT is a promising method of powering electrical devices, especially in environments where wired charging is inconvenient of even dangerous. Recently, the interest of WPT has been arise with the increase of mobile devices such as cell phones, PDAs, laptops, tablets, and other handheld gadgets equipped with rechargeable batteries has been widely spreading. In recent years, WPT technology has already been applied to tooth brushes and mobile phones. In addition, many researchers are interested in applying WPT technology to electrical vehicle, cordless zone, and biomedical application and are conducting research to realize it. The area where wireless power transmission technology is most needed is biomedical. Biomedical devices to be implanted in the body are most severely limited by their small volume and battery capacity limitations. WPT technology is the most suitable technology to solve this problem. However, power loss occurs during wireless power transmission, it is necessary to overcome this problem because the harmful effects on the human body. In this dissertation, two new power control techniques are introduced to increase the efficiency of wireless power transmission in biomedical systems. The first proposed technique is a technique for transmitting power more efficiently at a place where the transmission distance is long, the size of the device is small, the position of the device is not fixed, and the efficiency is very low like a capsule endoscopy. The second proposed technique is a power control technique which can increase the power transfer efficiency for applications with close distances for implanted biomedical devices under the skin like a cardiac pacemaker.

Chapter II presents a new power control technique to improve efficiency in magnetic resonance (MR)- WPT system for biomedical capsule endoscopy. Recently, capsule endoscopy technology has been developed and emerged as an alternative to small bowel endoscopy, gastroscopy, and colonoscopy, all of which cause discomfort to patients because of their relatively large-diameter and flexible cables. However, commercialized capsule endoscopy still suffers from limited battery capacity. Chapter II presents a theory for power control technique in MR-WPT system, along with its experimental verification. An MR-WPT system with a 9-mm-diameter receiver is implemented, which is small enough to fit in the current capsule endoscope. The proposed system improves the efficiency despite variations in the distance, angle, and displacement. The proposed system is found to have a low specific absorption rate, which demonstrated that it is safe to use in the human body.

Chapter III proposes power control technique for inductive power transfer (IPT) battery charging system using in-band communication that aims to minimize number of power stages and increase power transfer efficiency with low-cost hardware. Constant current and constant voltage mode are needed to effectively charge Li-ion batteries to ensure long life-span and maximum capacity utilization. These two charging modes require different feedback loops and circuitry, which increase system complexity and reduces efficiency. One approach is to use additional converter stages that ensure effective battery charging, but this introduces additional conversion losses, which decreases efficiency. The IPT system using proposed step charging method tracks the proper frequency to maintain the desired constant current or voltage for battery charging without the need for additional regulation circuits, and with minimized feedback control signal. In-band communication is used to send

feedback signal from secondary side to primary side of the IPT system, which enables effective feedback control without conventional wireless communication module. This power control technique is a technique to eliminate power loss in an unnecessary regulator. This technology is applicable to IPT using in-band communication and is suitable for implantable devices because it reduces receiver loss.

Contents

List of Figures

List of Tables

Nomenclature

WPT Wireless Power Transfer

WPC Wireless Power Consortium

IC Integrated Circuit

EV Electrical Vehicle

MR Magnetic Resonance

IPT Inductive Power Transfer

GI Gastro-Intestinal

LED Light Emitting Diode

ADS Advanced Design System

HFSS High Frequency Structure Simulator

ISM Industrial, Scientific and Medical

CENELEC European Committee for Electrotechnical Standardization,

ICNIRP International Commission on Non-Ionizing Radiation Protection,

IEEE Institute of Electrical and Electronics Engineers

SAR Specific Absorption Rate

EM Electro-Magnetic

CC Constant Current

CV Constant Voltage

SS Series-Series

SP Series-Parallel

PS Parallel-Series

PP Parallel-Parallel

MCU Micro-Controller Unit

PWM Pulse Width Modulation

Chapter I

Introduction

This chapter introduces fundamentals of wireless power transfer, including definition, history, basic mechanism, important parameters and classification of wireless power transfer (WPT). The application areas where WPT systems are used and why WPT is essential to biomedical are discussed. The technical challenges of WPT in biomedical applications are discussed and the technologies required to solve them are discussed.

1.1. Wireless Power Transfer

WPT is a breakthrough technology that provides energy to portable devices without the power line. With the remarkable progress being made recently, WPT technology has been attracting huge attention of researchers and industrial around the world. The concept of WPT traces back to the 19th century when means of transmitting electrical power wirelessly was being discovered.

In 19th century, Maxwell had published the famous equations in his "Treatise on Electricity and Magnetism" in 1873, which predicted that energy could be propagated though free space by electromagnetic waves form [1-1]. In 20th century, Nicola Tesla studied techniques of wirelessly transfer power and invented Tesla coil, which is first invention of WPT. However, there was no demands for WPT because of the period [1-2]. In world war II period, the applications such as the solar power satellite and high-altitude microwave powered aircraft are required, developed and expended [1-1]. In 2007, Marin Soljacic group proposed the technique of the middle-range WPT called magnetic resonance [1-3]. After published this technique, WPT area has been rapidly growing research area in various range of applications. In 2008, wireless power consortium (WPC), which is industrial standard of WPT, has been founded. WPC announced the first smart phones using Qi, which is low power specification logo, wireless technology. WPC's technology becomes most wide spread technology of WPT in mobile applications [1-4].

The motivation for wireless power comes complex and messy wires due to increase of the electrical devices, which is shown is Fig.1-1. Power supply line is the last remaining wire in mobile devices. Due to the fast development of the semiconductor fabrication and integrated circuit (IC), we own the large number of mobile electronics today. Nowadays, the mobile devices do not require wires for communication due to the development of wireless communication. There are demands for the convenience way to supply power to the mobile devices. WPT is promising technology that opens a new era of information technology without the power transferring wire. WPT is becoming the main concern of more and more research and development enterprises to eliminate the last wire. Recently, WPT technology has been applied to various fields such as mobile phone and tooth brush, and has been under studied to apply to electrical vehicle and biomedical application. Fig. 1-2 is an illustration of the field of wireless power transmission. Among many fields, biomedical is one of the most necessary fields for convenience and safety of patients equipped with biomedical devices.

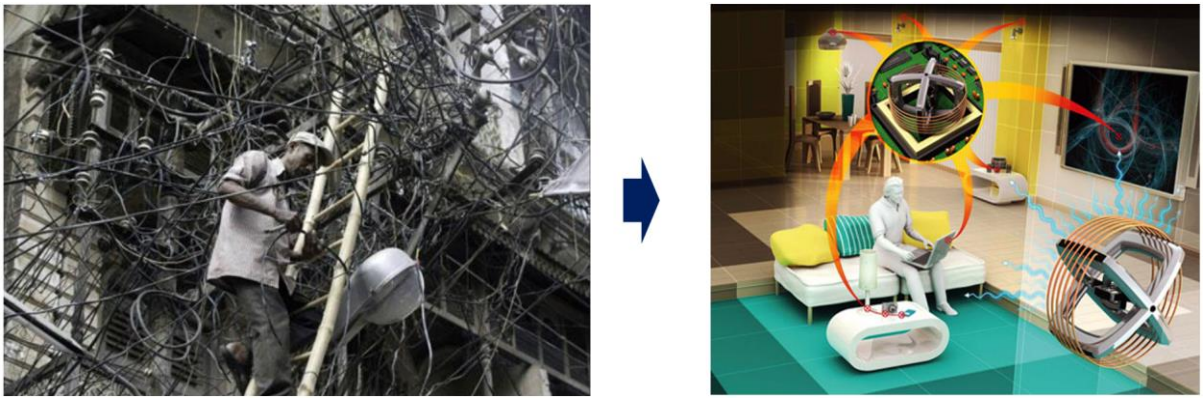

Fig.1-1. Illustration of wireless power transfer.

Fig. 1-2. Applications of WPT technology: cell phone, toothbrush, EV and biomedical devices.

1.2. WPT for biomedical application

Recently, a number of biomedical devices have been developed and commercialized to monitor patients' health and cope with emergencies in the development of electronic devices. The devices used for biomedical application are capsule endoscopy, gastric stimulator, glucose sensor, cochlear implant, cardiac pacemaker, insulin pump, etc., which is shown in Fig. 1-3.

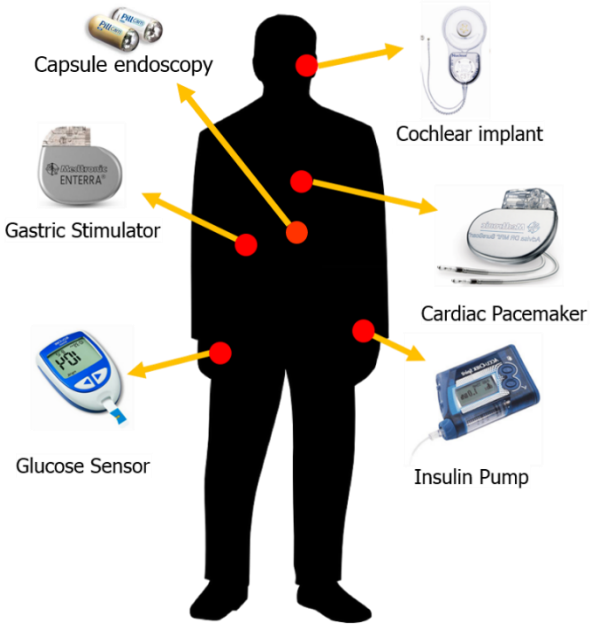

Fig. 1-3. Biomedical applications.

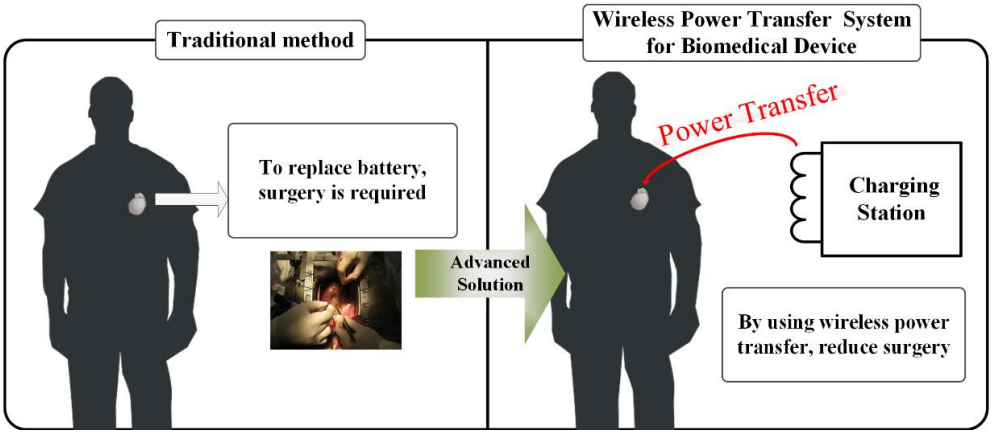

Fig. 1-4. The WPT technology is applied to biomedical application.

Patients are being assisted by biomedical devices, but there are still many inconveniences. First, the battery size is so large that it is uncomfortable to insert a foreign body into the human body. Especially for pacemakers, more than 50% of the devices are made of batteries. The second problem is the life of the battery. In the case of a pacemaker, the life span of the battery is about 8 to 10 years [1-5]. If the battery is discharged, an operation is required to replace the battery. This periodic operation causes pain and discomfort to the patient. The third problem is that devices such as capsuled endoscopy require more functions and efforts are being made to put them into small capsules, but they are limited by the battery capacity limitations. The best way to solve this is to combine WPT technology with biomedical application. This allows continuous charging regardless of battery life, thus avoiding unnecessary surgery, which is shown in Fig. 1-4. And, the size of the battery can be reduced. Therefore, WPT technology is a necessary technology for future biomedical applications.

1.3. Efficiency and Loss in WPT

The important factors to consider in applying wireless power transmission technology to biomedical are efficiency and loss. According to international commission on non-ionizing radiation protection (ICNIRP), when the temperature of the human body rises, the risk of cancer increases [1-6]. The factors that increase the human body temperature is discussed below.

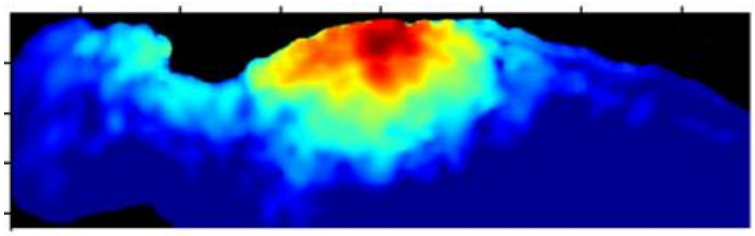

Fig. 1-5. SAR distribution when human body is exposed by electromagnetic field.

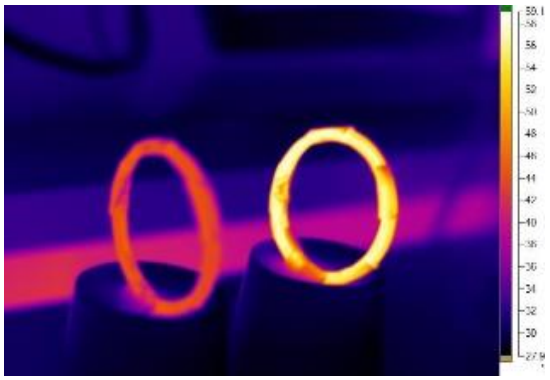

Fig. 1-6. Thermogram image of coils during power transmission.

The first thing to consider is specific absorption rate (SAR) for biomedical applications. SAR is the energy absorbed when electromagnetic wave is exposed to human body, which is shown in Fig. 1-5. The SAR is limited in each country because exposure to electromagnetic waves could cause the human body temperature to rise. When the wireless power transmission efficiency is low, the transmission power must be increased to radiate the minimum power required by each device, which increases the SAR. This can increase the temperature of the human body and is harmful to the human body. And, if the WPT efficiency is low, the energy lost will increase the temperature of the device, which again becomes a vicious cycle of lowering the efficiency. Fig. 1-6 shows the WPT coils temperature rise. When this low efficiency device is inserted into the human body and the temperature rises, it will have harmful effects on the human body. WPT efficiency enhancement technology is necessary to minimize human body temperature rise due to wireless power transmission loss. This dissertation proposes power control techniques for improving the efficiency of WPT technology in biomedical application.

1.4. Classification of WPT

Prior to dealing with efficiency in wireless power transmission, classifications of WPT technology are discussed in this chapter. The WPT is classified according to mechanism of power transfer method. The WPT scheme can be divided into ultrasonic transmission, microwave transmission, laser beam transmission, and magnetic coupled transmission.

1.4.1. Ultrasonic WPT

Ultrasonic is sound wave which is high frequency range from 20 kHz to several gigahertz. Recently, the research about mechanism and application of power ultrasonic technology has been highly getting attention and developed in related economy industry. Ultrasonic has been applied to many fields such as ultrasonic machining, processing technology, ultrasonic detecting and controlling technology. Ultrasonic power transmission utilizes piezoelectric effect and converse piezoelectric effect of piezoelectric material. The piezoelectric material can convert mechanical power into electrical power, or electrical power into mechanical power. When ultrasonic wave meets the piezoelectric material, it induces mechanical vibration of piezoelectric material and converted into electrical power. The research of ultrasonic WPT is focused on small power wireless charging system [1-7, 1-8]. Ultrasonic methods are very low efficiency and require precise alignment to achieve maximum efficiency. This technique is not suitable for biomedical application.

1.4.2. Laser beam WPT

The laser beam is coherent light beam capable to transport very high energies. Spatial coherence allows a laser to be focused to a tight spot. This makes it possible to efficiently send energy point to point in a line of sight. The theory of laser power transmission is simple and like common laser generator and power source. Power source is to provide necessary power to laser generator. The power converted into laser power and send it out. Laser receiving equipment is to receive laser from laser generator and convert it into electrical power. This is same mechanism with solar cell. The research is spotlighted by space based solar power and satellite solar power system. NASA introduced in 2003 a remote-controlled aircraft wirelessly powered by a laser beam and a photovoltaic cell which is infra-red band sensitive solar cell, shown in Fig. 1-7 [1-9]. Laser-based wireless power transmission technology is not suitable for biomedical applications in a way that is highly harmful to the human body, although it achieves high efficiency.

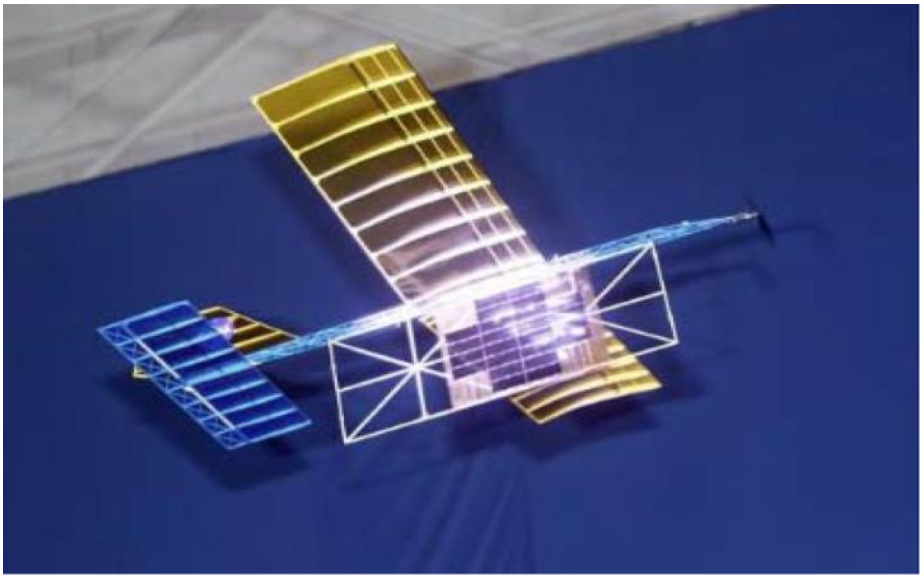

Fig. 1-7. Airplane driven by laser.

Fig. 1-8. Microwave power was fed to the airplane with rectennas [1-10].

1.4.3. Microwave WPT

Microwave is one kind of electromagnetic wave, whose wavelength is from 1 mm to 1 m, frequency from 0.3 GHz to 300 GHz. The investigation of long range power delivery with microwaves is carried out with endeavors [1-11], the efficiency or power delivery is still quite low that is not sufficient to fully charge typical industrial electronic. In addition, when using these far-field techniques, any obstruction such as metal or conducting materials in the transfer path is not allowed. It is dangerous for human bodies or other organisms which in the energy transfer path according to IEEE standard for radio frequency electromagnetic fields [1-12]. Such power transfer is relatively suited to very restrict applications unless they are used in military or space explorations which are less regulated environments. The microwave method is similar to the laser method. The microwave method is similar to the laser method. It is not suitable for biomedical because it is harmful to human body

1.4.4. Magnetically coupled method WPT

The magnetically coupled method WPT technologies are classified into two categories. The first WPT technology is the inductive power transfer (IPT) technology. The second WPT technology is magnetic resonance (MR)-WPT, which is a medium-range wireless power transmission. This chapter discusses the characteristics of the two WPT technologies.

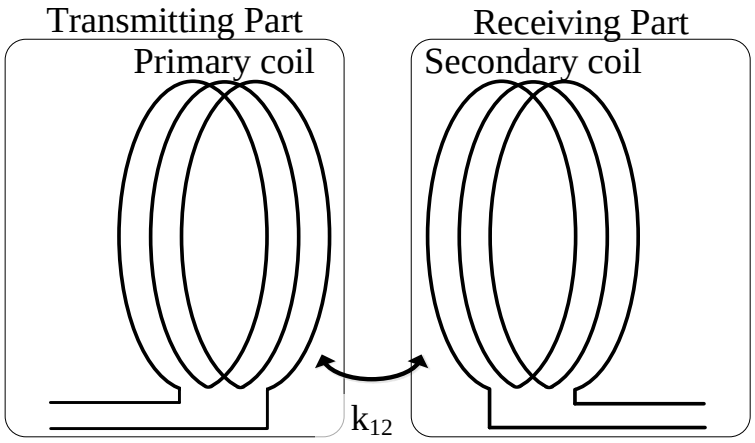

Fig. 1-9. Coil structure of IPT technology.

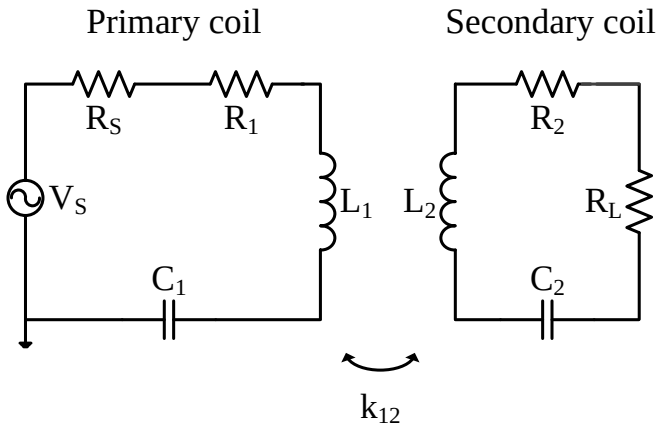

Fig. 1-10. Equivalent circuit of IPT.

Figure 1-9 shows the coil structure of the IPT method. In the case of IPT, there are two coils, and the power is transmitted due to the coupling of the two coils. Fig. 1-10 shows the equivalent circuit of IPT. The IPT has two resonant systems. Usually IPT has a low Q-factor due to source resistance and load resistance. The detail of Q-factor is described in the next chapter. IPT usually transmits power at a short distance, and the transmission distance is short due to a low Q-factor, but it is a good to control the transmission power. It has high efficiency because it transmits at close range.

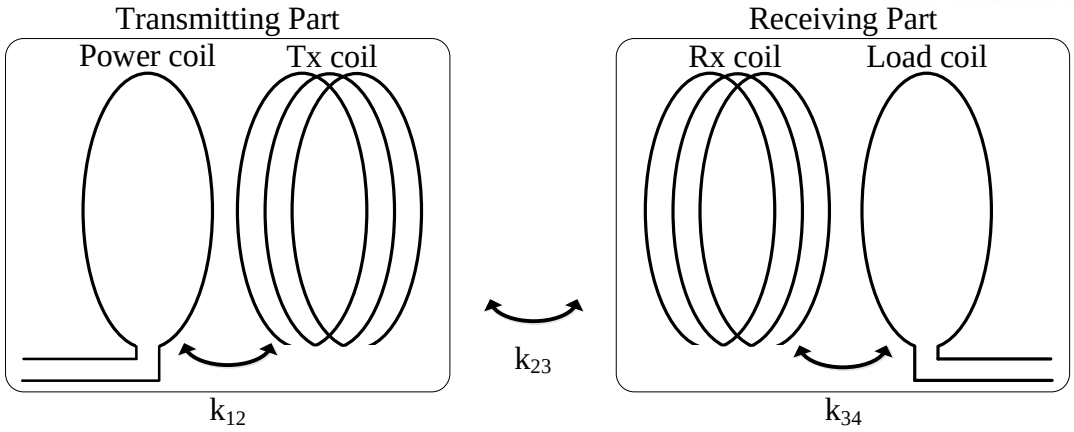

Fig. 1-11. Coil structure of MR-WPT technology.

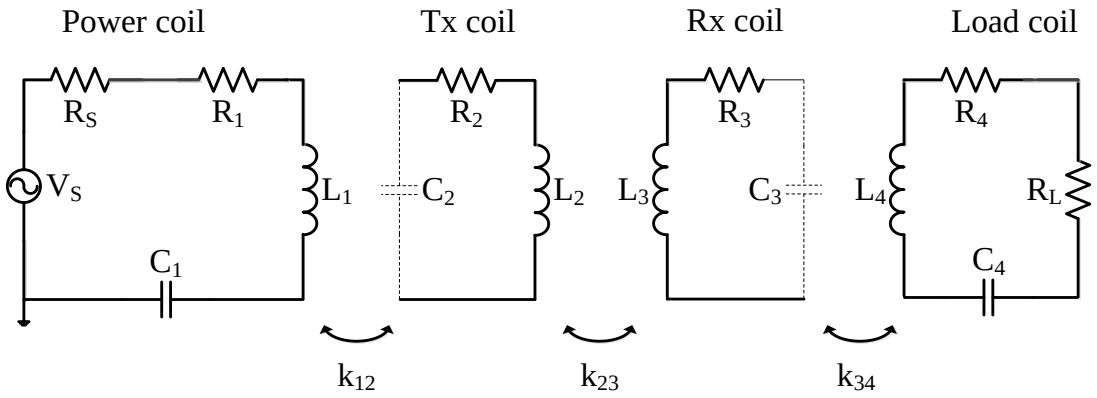

Fig. 1-12. Equivalent circuit of MR-WPT.

Figure 1-11 shows the coil structure of the MR-WPT method. The MR-WPT consists of four coils. MR-WPT has two separate Tx and Rx coils for high efficiency. Power coil is connected to the source, which is strongly coupled with Tx coil. Load coil is connected to the load, which is strongly coupled with Rx coil. The power coil and Tx coil are a pair of transmitting side coils. The load coil and Rx coil are a pair of receiving side coils. The Tx and Rx coils are usually designed to cut off both ends of the wire and exhibit self-resonance characteristics. Fig. 1-12 shows the equivalent circuit of MR-WPT. A capacitance for LC resonance in a resonant coil is parasitic capacitance. The parasitic capacitance has a very low value, which means that the Q-factor of the Tx and Rx resonators is very high. Because of its high Q-factor, it has the advantage of being able to transmit at a distance greater than IPT. However, since the efficiency is relatively low, it is necessary to study the efficiency improvement.

1.5. Basic principle

The Fig. 1-13 is a schematic diagram for explaining the magnetic coupled wireless power transmission. It consists of two coils, coil 1 is transmitter and coil 2 is a receiver. The theory behind wireless power transfer is detailed in the Maxwell's equations:

$$\nabla \cdot \mathrm{D} = \rho \tag{1.1}$$

$$\nabla \cdot \mathrm{B} = 0 \tag{1.2}$$

$$\nabla \times \mathrm{E} = -\frac{\partial B}{\partial t} \tag{1.3}$$

$$\nabla \times \mathrm{H} = \mathrm{J} + \frac{\partial D}{\partial t} \tag{1.4}$$

The (1.3) equation indicates that the curl of electric field is proportional to the rate of change of the magnetic flux. This is called Faraday equation. The (1.4) equation indicates that the curl of magnetic field is proportional to the electrical current. This is called as Ampere's law. Therefore, if a time-varying electric current is generated in coil 1, the time-varying current will induce a time-varying magnetic field. This magnetic field induces a time-varying electric field, or an AC voltage across a receiving circuitry. Due to the time-varying electric field, a magnetic field is generated in the opposite direction of the magnetic field due to coil 1. Based on these laws, Coils can generate/receive a time-varying magnetic field in free-space. It shall be emphasized is not based on the direct transfer of energy using propagating electromagnetic wave. Magnetic coupled method is a near-field method, whereas the use of propagating electromagnetic wave, like transmission of microwave power through an antenna, is a far-field method. This method is base mechanism of the WPT of used in current era.

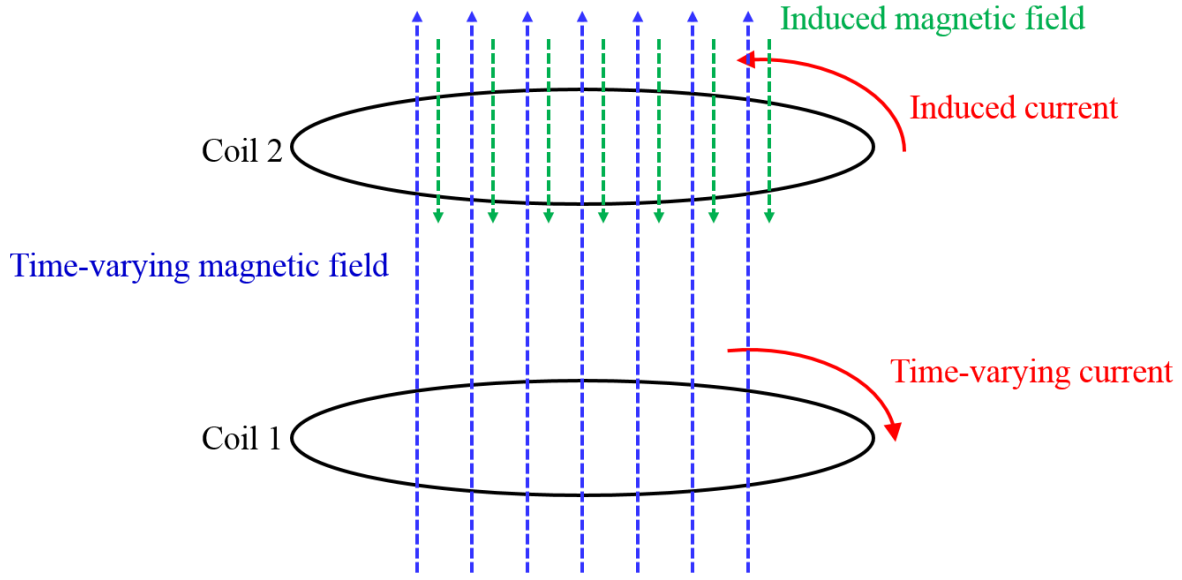

Fig. 1-13. Basic principle of wireless power transfer.

1.6. Basic parameters in WPT

This chapter describes the important parameters used in magnetically coupled WPT technology. Q-factor representing the amount of power transmission that can be transferred is described. And the mutual inductance and coupling coefficient that explain the degree of coupling is described in this chapter.

1.6.1. Quality factor

The quality factor (Q-factor) is a dimensionless parameter that describes the bandwidth of resonator relative to its center frequency. High Q-factor means a low power loss compared to the stored power of resonator. In WPT technology, high Q-factor system indicated that system can transfer power more efficiently than low Q-factor system. Thus, this value is used as a figure of merit of the wireless power transfer coils. In RLC circuit, the quality factor is defined as

$$\mathrm{Q} = \frac{1}{R}\sqrt{\frac{L}{C}} = \frac{\omega L}{R} = \frac{1}{\omega RC} \tag{1.5}$$

where Q is quality factor, L is inductance, C is capacitance and R is resistance of RLC resonator. The Q-factor value is between 0 and infinite. In Fig. 1-14, Quality factor characteristic is described. The Q-factor is important parameter when design IPT and MR-WPT system. In IPT system, high Q-factor is not required, because power transfer distance is very close and coupling coefficient is very high. The high coupling coefficient system efficiency is high enough in close distance. In this system, high quality factor increases the selectivity of frequency, which makes the system complex. In MR-WPT system, high Q-factor is required, because power transferring distance is longer than IPT. The coupling coefficient is very lower than IPT system. Thus, MR-WPT adopts high Q-factor RLC network to increase power efficiency.

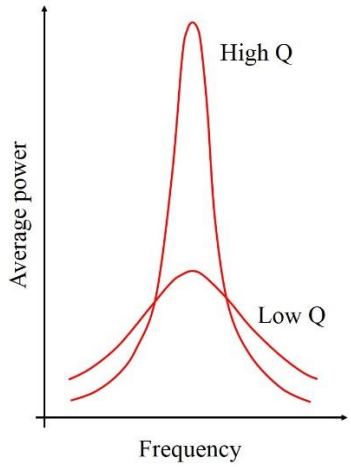

Fig. 1-14. Quality factor characteristic.

1.6.2. Mutual inductance and coupling coefficient

Mutual inductance occurs when the change of current in one inductor induces time-varying magnetic flux, which induces a voltage in nearby inductor. This is important mechanism of WPT. The mutual inductance can be express as

$$v(t) = M\frac{di(t)}{dt} \tag{1.6}$$

where v(t) is time-varying voltage and i(t) is time-varying current. M is mutual inductance. The unit of mutual inductance is henry (H). The mutual inductance between two inductors can be express as

$$M = k\sqrt{L_1 L_2} \tag{1.7}$$

where, k is coupling coefficient and L_1 and L_2 are inductance of the coils. The coupling coefficient is dimensionless value that indicates coupled decree between coils. The coupling coefficient is defined the range as $0 \leq k < 1$. But some define it as $-1 < k < 1$. Negative k means phase inversion of the coils connection [1-13] and the direction of the winding [1-14].

Based on Biot-Savart law, magnetic flux density B_o of the coils can be derived from follow:

$$B_o = \oint dB_o = \frac{\mu_0}{4\pi} I_o \oint \frac{d\vec{s}\times\hat{r}}{|\vec{r}|} = \frac{\mu_0 I_o r_0^2}{2(r_0^2+z^2)^{3/2}} \tag{1.8}$$

where $I_o dl$ is the infinitesimal current source line on the o loop, and μ_o is the permeability of the free space. The z is the geometric parameter in Fig. 1-15. Faraday's law and Lenz's law imply that a time-varying current in the o loop (I_o) results in a time variation of the magnetic flux through the i loop ($\Phi_{i,o}$). With equation (1.8), mutual inductance derived by equation (1.8) is express as [1-15]

$$M = \frac{\mu_0 \pi r_0^2 r_i^2}{2(r_0^2+z^2)^{3/2}} \tag{1.9}$$

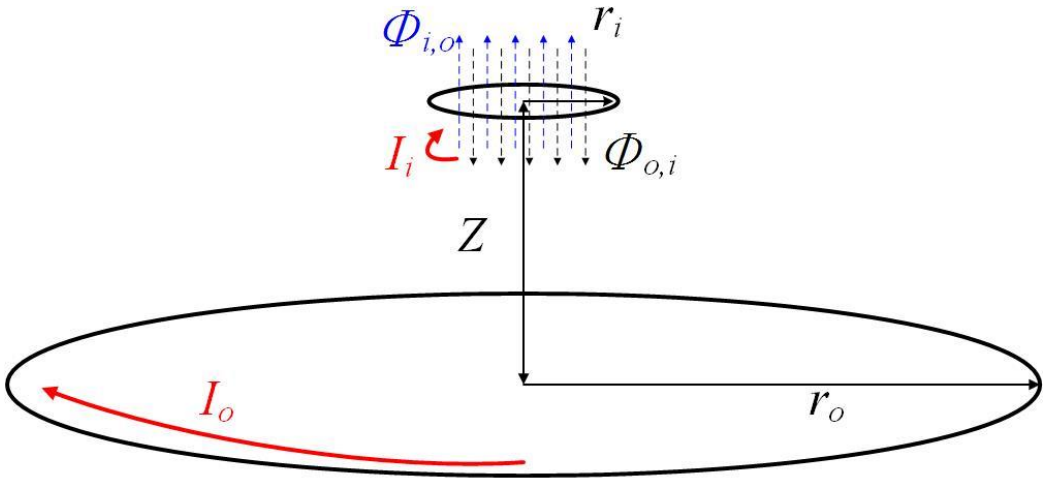

Fig. 1-15. Simple magnetic resonance wireless power transfer coils with geometric and electrical factor.

1.7. Technical challenges and approaches

1.7.1. Efficiency degradation depending on geometric value changes

Fig. 1-16 shows typical arrangement of the magnetically coupled coils during power transfer. The geometric parameters in Fig. 1-16 are compared to diameter D of the large coil. L_1 and L_2 are inductance of the coils. The z value is axial distance between L_1 and L_2. D_2 is the diameter of the coil L_2. Fig. 1-17 shows the relationship among the geometric parameters. The power transfer efficiency is maximum constant value at $z/D < 0.1$ condition. When z/D is larger than 1, efficiency is dramatically decreased. When D_2 is 30% size of D, efficiency drops dramatically. The efficiency is higher than 90% at D_2/D is higher 0.5. These characteristics show the limitation of power transfer distance [1-4]. When wireless power transmission is applied to biomedical applications, a reduction in efficiency due to small D_2/D, because of the small size biomedical devices, cannot be avoided.

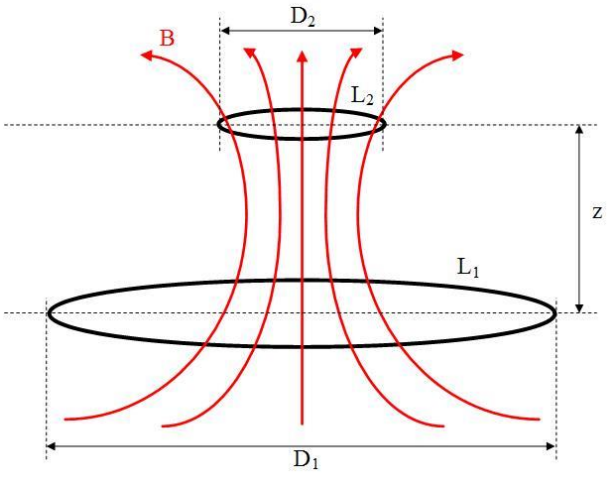

Fig. 1-16. Magnetically coupled coils during power transfer.

Additionally, there is a problem of low efficiency due to varied distance, displacement and angle and small size receiver. This limitation is caused by the coupling coefficient degradation, which is shown is Fig. 1-18. The coupling coefficient indicates magnetic flux affect to each coil. Low coupling coefficient means low magnetic flux to the receiver coil and low efficiency of power transfer. The coupling efficient is variable of the geometric values and size ratio of the coils. The maximum coupling coefficient is decided by the ratio of the resonator coils size. When $D_2/D < 0.3$, the maximum k value is below 0.1.

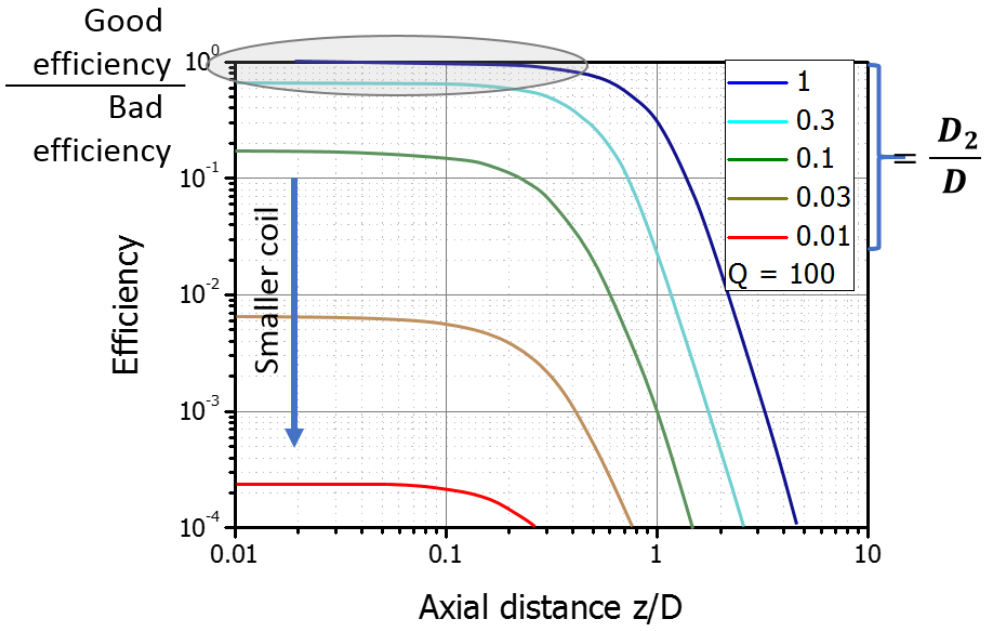

Fig. 1-17. Efficiency for an inductive power transfer system consisting of loop inductors depending on axial distance z with size ratio as parameter.

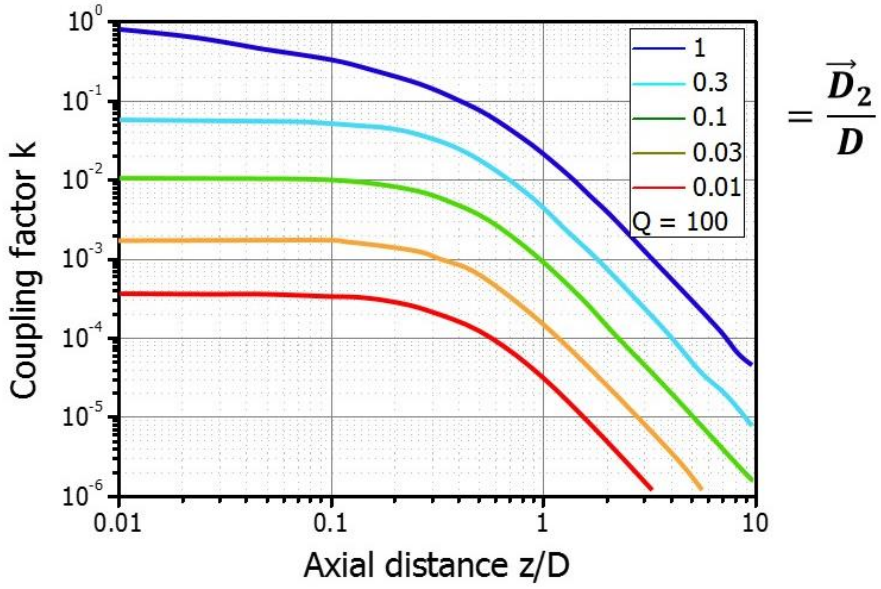

Fig. 1-18. Coupling coefficient depending on size of resonators and distance between coils.

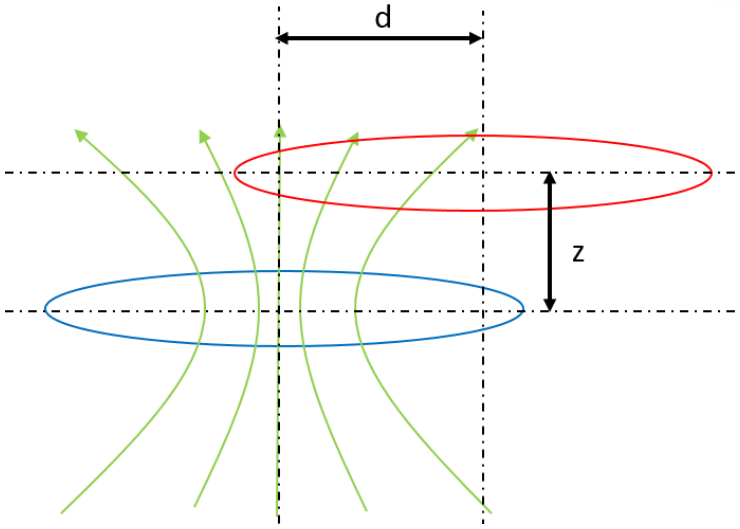

Fig. 1-19. Magnetically coupled coils during power transfer depending on distance and displacement.

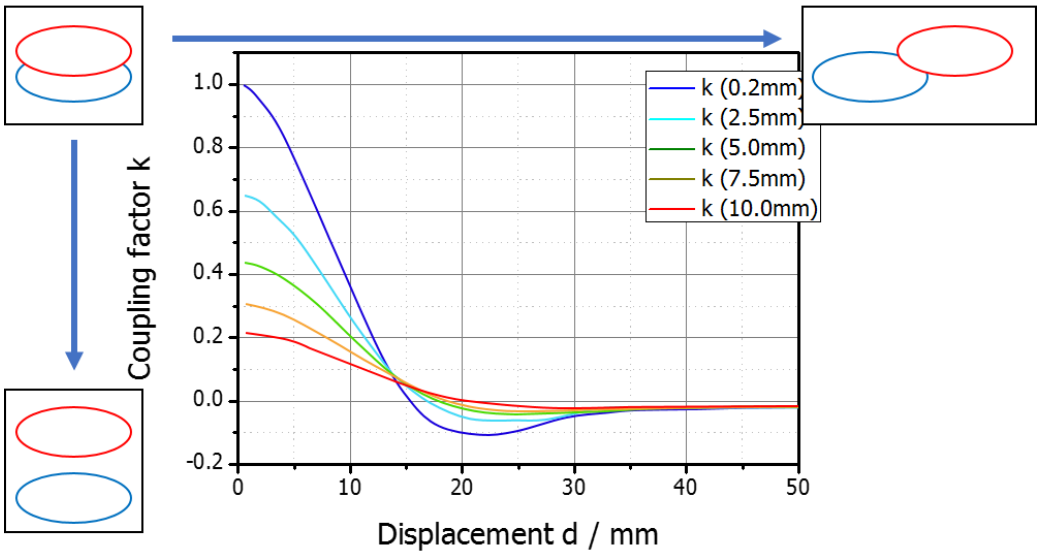

Fig. 1-20. Coupling coefficient depending on the distance and displacement.

Figure 1-19 shows the displacement setup of the coils. Fig. 1-20 shows the degradation of the coupling coefficient depending on the displacement. The coupling coefficient is dramatically degraded when resonators are not aligned at same axis. Fig 1-21 shows the efficiency degradation of the WPT system depending on distance, angle misalignment and displacement. These are simulated result by HFSS. The efficiency is gradually degraded distance between resonator is increased, which is shown in Fig. 1-21(a). In Fig. 1-21(b), the efficiency is decreased exponentially as become Tx and Rx coils are vertical. In Fig. 1-21(c), the efficiency is dramatically degraded after 0.75 displacement (1 is 4 times lager distance than diameter of the Rx coil).

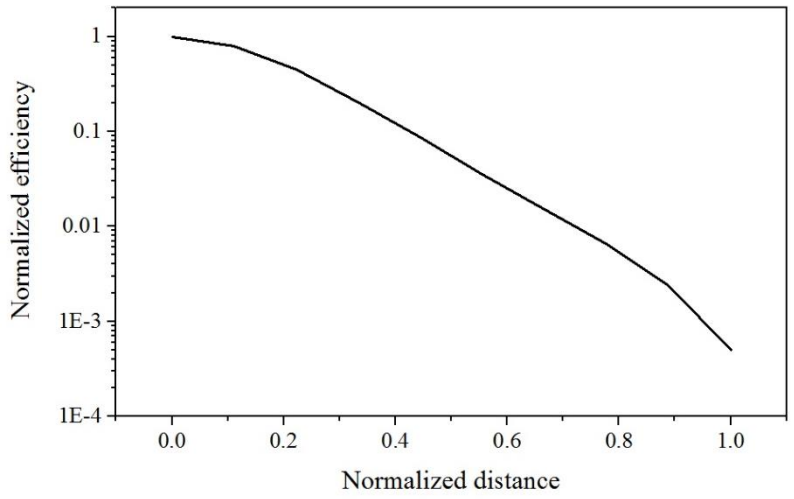

(a)

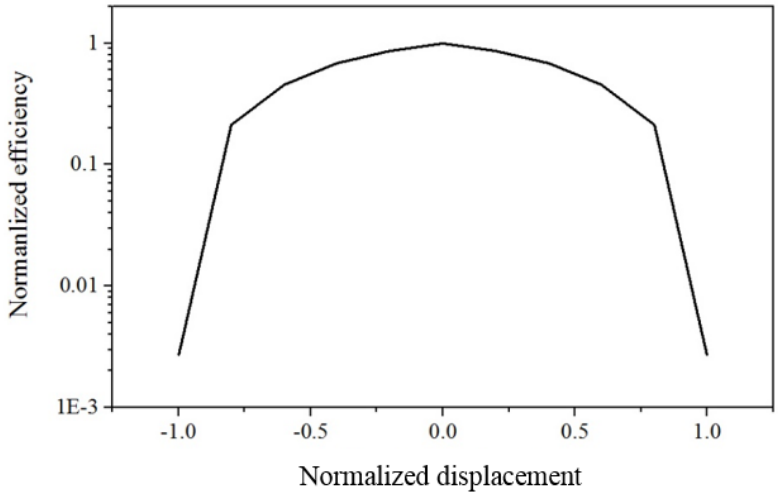

(b)

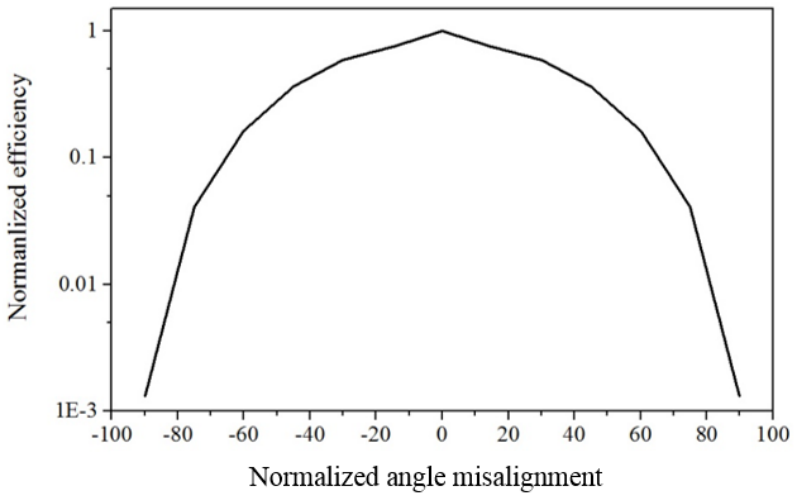

(c)

Fig. 1-21. Simulated MR-WPT efficiency result in geometric variable change environment, depending on (a) distance, (b) displacement, (c) angle misalignment.

To overcome this limitation, there are a lot of research to increase the WPT system transfer range and efficiency [1-16~19]. In work [1-16, 1-17], additional resonators are used as repeater to enhance transfer range and efficiency. However, these works did not consider the change of the transfer distance. Work [1-18] present a technique of improving the efficiency when the distance between the resonator coils by changing the coupling coefficient k_{12} and k_{23}. This technique does not require additional matching network. However, this technique is limited to the symmetric Tx and Rx coils system. Adjusting k_{34} is not suitable for applications with small devices like biomedical application. Work [1-19] proposed and demonstrate the efficiency improvement of MR-WPT between asymmetric resonators with different sizes with theoretical analysis. Nonetheless, this work does not solve the angle misalignment and displacement. In this dissertation, power control technique to increase efficiency in WPT system is presented in the environment of geometric position changes.

1.7.2. Load variation of battery

The next technical issue is load variation of battery. To charge rechargeable battery, constant current mode and constant voltage mode are required for longer life time, large capacity. Fig. 1-22 shows battery charging graph and equivalent resistance of battery. In CC mode, battery voltage and equivalent resistance increased continuously. In order to meet the CC mode condition, the charging power must be increased to match the battery condition. In CV mode, battery charging voltage have to be fixed at maximum battery voltage. To meet the CV mode condition, the voltage must be constant, so the current continues to decrease, and the charging power continues to decrease. To charge the battery, WPT system must support CC/CV mode function.

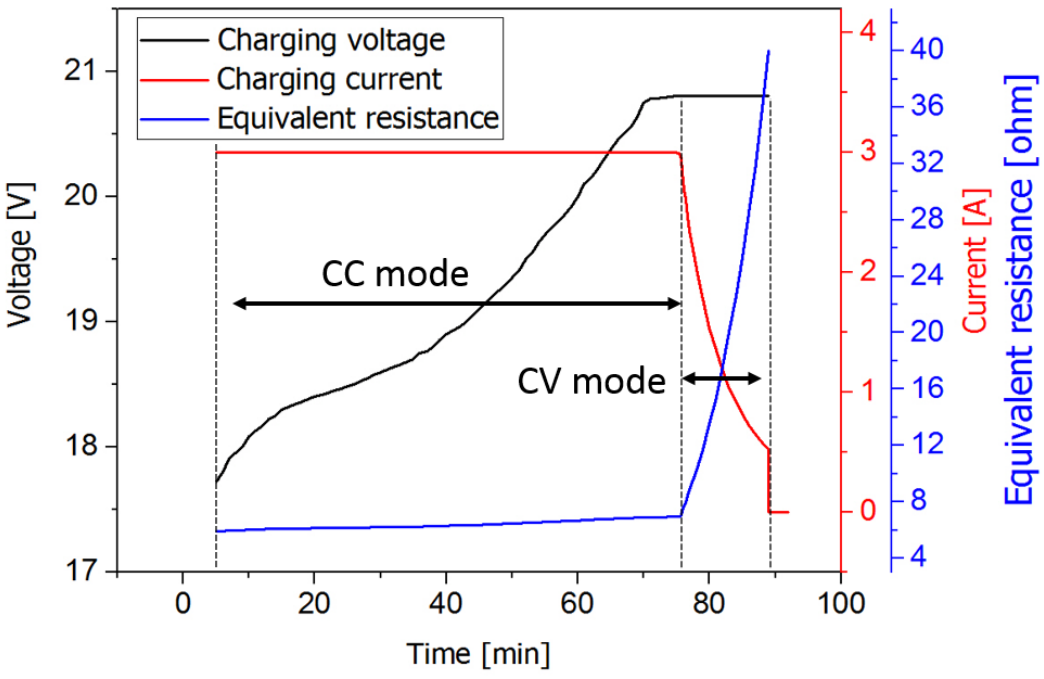

Fig. 1-22. Battery charging graph and equivalent resistance of battery.

Many working group researched to improve efficiency. A new magnetic design for an IPT pad called the bipolar pad (BPP) was introduced by [1-20]. And Zero voltage switching technique was introduced by [1-21]. Works in [1-20~22] used battery charger circuit after rectifier to realize CC/CV mode. Additional power stages decrease total efficiency. “Hybrid topology compensation technique” was introduced by [1-23]. To meet CC mode condition, CLC topology was used. To meet CV mode condition, LCL topology was used without battery charger. Although, this topology reduces the power stages, CC/CV mode is working with well impedance matched conditions. This is sensitive to alignment between TX and RX. “IPT using regulator and FM” technology uses in-band communication for feedback system was introduced by [1-24, 1-25]. Frequency modulation and LDO regulator were used for voltage regulation. Regulator causes about 250mW (5%) power loss. In this dissertation, power control technique to reduce regulator loss power in IPT system with in-band-communication is presented.

1.8. Thesis contributions

This dissertation focuses on the power control techniques in wireless power transfer system to control battery charging voltage and current, and to maximize power efficiency depending on change of geometrical position for biomedical applications.

- Due to a resonant coupling nature of the WPT system, for the most efficient power transmission, there is an optimum range between a power coil and a transmitting coil for a fixed distance between the transmitting and receiving coils. In this dissertation, an equivalent circuit model for a WPT system via magnetic resonance will be derived and analytically solved to improve the power transfer efficiency depending on change of geometric position, such as distance, angle and displacement.

- To charge battery, CC/CV mode in WPT are required without extra battery charger block such as DC-DC converter or regulator type charger. However, theses extra power cause power efficiency. In this dissertation, step charging method is proposed to charging battery in IPT system using in-band communication. Theoretical analysis is studied for frequency modulation and in-band communication in IPT system. Experimental result is followed to demonstrate proposed technique.

Chapter II

Power control technique for variable geometric position in wireless power transfer system

2.1. Background

Visualization of the human gastro-intestinal (GI) tract, upper small intestine, and colon became possible after the development of optical fiber endoscopy. Generally, flexible wire endoscopy does not present significant problems. However, small intestine endoscopy, gastroscopy, and colonoscopy induce discomfort among patients due to the large-diameter flexible cables needed to withstand the push force, and which carry a video signal and power through optical fiber and wire. In addition, visualization in some GI tracts is still difficult using flexible wire endoscopy [2-1]. For this reason, through the rapid progress of semiconductor and communication technologies, capsule endoscopy has arisen as a new advanced technology to address the problems with flexible wire endoscopy, as illustrated in Fig. 2-1 [2-2, 2-3].

In most bio-medical sensor networks, the limit on the amount of power that can be supported by the embedded battery presents a problem. Implantable devices such as a glucose sensor, implantable defibrillator, retinal display, and gastric stimulator have to be taken out periodically via surgery to change the battery, causing patients great discomfort and the potential for complications, just as in other procedures. Recently, capsule endoscopy has also encountered the power shortage problem in the GI tract because of the demand for higher resolution video and the increase in the number of integrated functions [2-1, 2-4, 2-5].

Capsule endoscopy consists of several parts, including vision, control, and data transmission components, in a capsule that is typically 11 mm in diameter by 25 mm in length. Although different amounts of energy are consumed, depending on the components, it is clear that each part consumes electrical energy. Vision processes, the first element of capsule endoscopy, utilize a CMOS image sensor, light emitting diode (LED) illuminator, and processor. In the previously used capsule endoscopy products, the data rate of the images was a few Mbps because of the limitation of the technology in this field [28]. However, with increasing consumer demand and developing technologies, the frame rate and quality of images have improved. The HD CMOS image sensor provides up to 30 fps at 1920 × 1080 pixels per frame at a data rate of 78 Mbyte/s [2-6]. It consumes almost 40 mW of power. The LED illuminator should also turn on more frequently, and the processor consumes about 10 mW. With four LED illuminators in use, the total power consumption of the vision component is more than 90 mW.

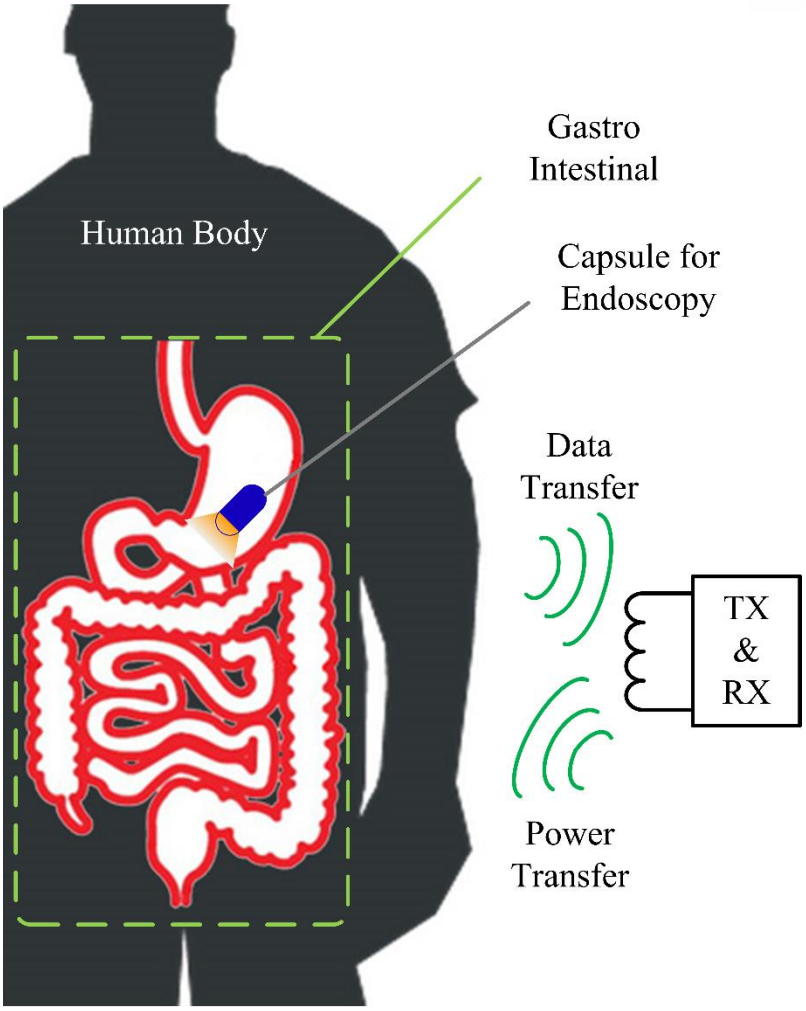

Fig. 2-1. Concept of capsule endoscopy with wireless power transfer in gastro-intestinal (GI) tract of human body.

With respect to the control element, movement is an additional advanced function in demand. In terms of the current capsule endoscope market, the locomotion controls and actuators have not been commercialized. These locomotion controls and actuators are considered to be essential parts of future capsule endoscopes for fast and accurate diagnosis [2-7~9]. However, this increased benefit corresponds to increased power consumption. For example, locomotion requires more than 300 mW, while actuators consume more than 200 mW. Fortunately, these control features are only used during a short period, as opposed to being used for the entire operating time.

Finally, the data transmission part consists of a transmitter and receiver. This part consumes approximately 5 mW, which is less than the other two parts. However, the transmitter is used during the entire procedure, and its total power consumption can accumulate to a significant number that is comparable to the locomotion control and actuators. The receiver is utilized less than the transmitter, but its power consumption is almost the same as that of the transmitter.

Module	Required Power	Duty time
CMOS Image Sensor	40 mW	70-100%
LED Illuminator	80 mW	70-100%
Processor	10 mW	70-100%
Locomotion	>300 mW	3-5%
Actuator	>200 mW	1-2%
Transmitter	5 mW	90-100%
Receiver	5 mW	1-80%

Table. 2-1. Power consumption table of the main modules embedded in future for capsule endoscopy.

Power consumptions for future capsule endoscopy according to functions are described in Table. 2-1. Since the total power consumption greatly depends on the power consumed in the control parts, it is not trivial to estimate its exact value. A rough estimate is approximately 300 mW. This value is quite high considering the typical capacity of commercially available batteries [2-10]. As shown in the above, the required functions are increasing, but the battery area is getting smaller due to the limited volume. So WPT technology is a necessary for capsule endoscopy. However, digestive tract is positioned quite deep position compared to capsule size. Therefore, long distance WPT is required. The most suitable WPT structure for capsule endoscopy is MR-WPT. Because, MR-WPT can transfer power at longer distance compared to IPT method. However, when the coil size is small, the efficiency is low. MR-WPT efficiency is degraded depending on the misalignment of angle and displacement, so it is necessary to improve the efficiency in this condition.

This chapter presents a power control technique to track the high transfer efficiency of an MR-WPT system with variations in the relative distance, angle, and axial misalignment between asymmetric transmitting and receiving parts. The following sections present the new theoretical models, and then show how the proposed work was verified using measured experimental results. After that, the effects on the transfer efficiency of biological tissue blocking the proposed MR-WTP system and the specific absorption rate (SAR) are analyzed.

2.2. WPT model analysis

In this section, circuit and electromagnetic analyses are performed to define the essential model parameters for the design and present methods to overcome efficiency degradation. The circuit analysis focuses on the parameters affecting the coupling coefficient of the MR-WPT system. The electromagnetic analysis shows how the coupling coefficient is affected in terms of the dimensional parameters such as the distance and angle, which make the MR-WPT system controllable.

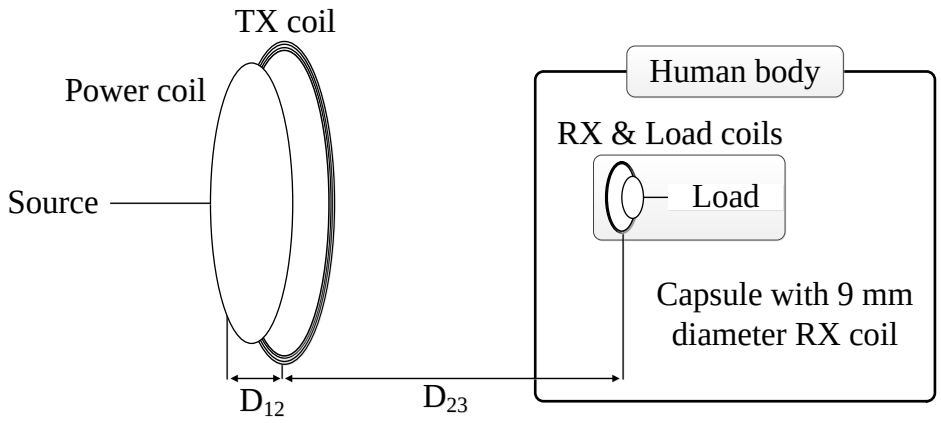

Fig. 2-2. Diagram model of the wireless power transfer system for capsule endoscopy.

2.2.1. Transfer characteristic analysis

A strongly coupled MR-WPT system consists of four coils. The proposed model of the MR-WPT system for capsule endoscopy, as illustrated in Fig. 2-2, consists of a power coil, transmitting coil (TX coil), receiving coil (RX coil), and load coil. The power coil is connected to a source outside of the human body. The load coil is connected to a capsule endoscopy system and provides additional power beyond the integrated battery. The TX and RX coils are called resonators, which are designed to resonate at the same frequency and have a high-quality factor with high inductance and low capacitance.

Figure 2-3 shows the equivalent circuit model of the four-coil MR-WPT system to analyze the maximum transfer efficiency condition. The circuit consists of four separate circuits. These circuits are connected via a magnetic field, which can be characterized by coupling coefficients k_{12}, k_{23}, and k_{34}. The coupling coefficient has a value between 0 and 1, which can be expressed as follows:

$$k_{xy} = \frac{M_{xy}}{\sqrt{L_x L_y}} \tag{2.1}$$

where M_{xy} is the mutual inductance between the "x" and "y" coils; and the parameters of each circuit are characterized by the resistance R_x, inductance L_x, and capacitance C_x.

This circuit model offers an effective way to analyze the characteristics of the proposed system. First, by applying Kirchhoff's voltage law to this model, the relationship between the currents through each coil and the voltage applied to the power coil can be expressed using the following matrix.

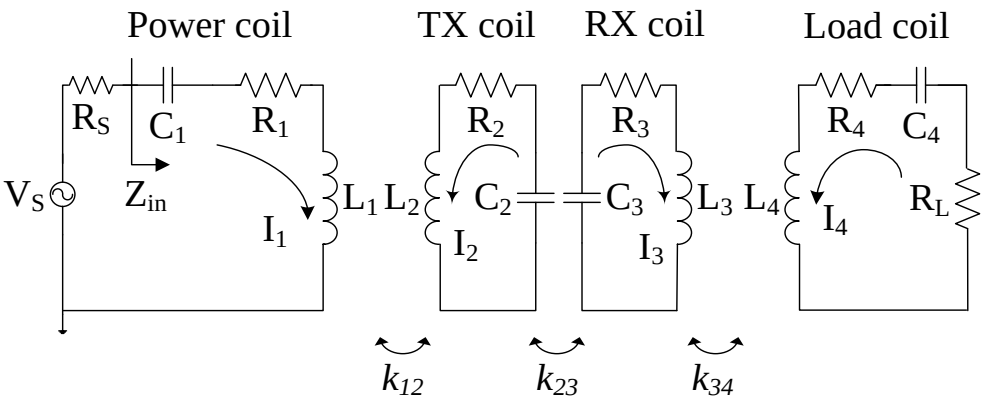

Fig. 2-3. Equivalent circuit model of a magnetic resonance wireless power transfer (MR-WPT) system.

$$\begin{bmatrix} I_1 \\ I_2 \\ I_3 \\ I_4 \end{bmatrix} = \begin{bmatrix} Z_1 & j\omega M_{12} & 0 & 0 \\ j\omega M_{12} & Z_2 & j\omega M_{23} & 0 \\ 0 & j\omega M_{23} & Z_3 & j\omega M_{34} \\ 0 & 0 & j\omega M_{34} & Z_4 \end{bmatrix}^{-1} \begin{bmatrix} V_s \\ 0 \\ 0 \\ 0 \end{bmatrix} \tag{2.2}$$

where Z_1, Z_2, Z_3, and Z_4 are the loop impedances of the four coils. These terms can be expressed as follows:

$$\begin{aligned} Z_1 &= R_S + R_1 + j(\omega L_1 - 1/\omega C_1) \approx R_S \\ Z_2 &= R_2 + j(\omega L_2 - 1/\omega C_2) = R_2 \\ Z_3 &= R_3 + j(\omega L_3 - 1/\omega C_3) = R_3 \\ Z_4 &= R_L + R_4 + j(\omega L_4 - 1/\omega C_4) \approx R_L \end{aligned} \tag{2.3}$$

where $j(\omega L_x - 1/\omega C_x)$ is zero at the resonance condition, and we assume that $R_S+R_1 \approx R_S$, and $R_L+R_4 \approx R_L$ because $R_S \gg R_1$ and $R_L \gg R_4$. The currents in the power and load coils are expressed by 4).

$$I_4 = \frac{j\omega^3 k_{12}k_{23}k_{34}L_2L_3\sqrt{L_1L_4}}{(R_SR_2 + \omega^2k_{12}^2L_1L_2)(R_LR_3 + \omega^2k_{34}^2L_3L_4) + R_SR_L\omega^2k_{23}^2L_2L_3} V_S \tag{2.4}$$

The efficiency of the WPT system can be expressed by the following equation:

$$\eta = \frac{P_{out}}{P_{in}} = \frac{V_L^2 / R_L}{V_S^2 / 4R_S} = |S_{21}|^2 \tag{2.5}$$

where η is the efficiency of the MR-WPT system; and Pin and Pout are the source power from the power coil and delivered power at the load coil, respectively. V_L and V_S are the voltages applied to the load and source, respectively. R_L and R_S are the port reference impedances with 50 Ω. This system model can be considered to be a two-port network. The S-parameter is a commonly used figure of merit for a given WPT system. S_{21} indicates the power transfer efficiency, which is given by $|S_{21}|$, the square magnitude of S_{21}. The S_{21} parameter is calculated as follows:

$$S_{21} = 2\frac{V_L}{V_S}\sqrt{\frac{R_S}{R_L}} \tag{2.6}$$

2.2.2. Mutual inductance depending on geometric factors

The magnitude of $|S_{21}|$ can be expressed by solving (2.4) and (2.6).

$$\begin{aligned} |S_{21}| &= 2\frac{V_L}{V_S}\sqrt{\frac{R_S}{R_L}} \\ &= \frac{2\omega^3 k_{12}k_{23}k_{34}L_2L_3\sqrt{L_1L_4}\sqrt{R_SR_L}}{(R_SR_2+\omega^2k_{12}^2L_1L_2)(R_LR_3+\omega^2k_{34}^2L_3L_4)+R_SR_L\omega^2k_{23}^2L_2L_3} \end{aligned} \tag{7}$$

The relationship between the transfer efficiency and coupling coefficient is analyzed using the circuit models, and the following demonstration focuses on the relationship between the coupling coefficient and geometric factors. In Fig. 2-4, a concentric resonator pair of single-turn loops with radii r_x and r_y ($r_x \gg r_y$), vertical displacement z, and angle θ between the y loop surface plane and plane parallel to the x loop is presented [2-11]. The Biot–Savart law leads to an expression for the magnetic flux density B_x at a field point r (at height z above the center of the loop axis) that is induced by the x loop:

$$\boldsymbol{B}_x = \int_x d\boldsymbol{B}_x = \frac{\mu_o}{4\pi} I_x \int_x \frac{d\boldsymbol{l}\times\boldsymbol{r}}{|\boldsymbol{r}|} = \frac{\mu_o I_x r_x^2}{2\left(r_x^2 + D_{xy}^2\right)^{3/2}} \tag{2.8}$$

where $I_x dl$ is the infinitesimal current source line on the x loop, and μ_o is the permeability of the free space. Faraday's law and Lenz's law imply that a time-varying current in the x loop (Ix) results in a time variation of the magnetic flux through the y loop ($\Phi_{y,x}$). The minus sign in (2.9) is an indication that the EM field is in such a direction as to produce a current whose flux reduces the magnitude of the EM field.

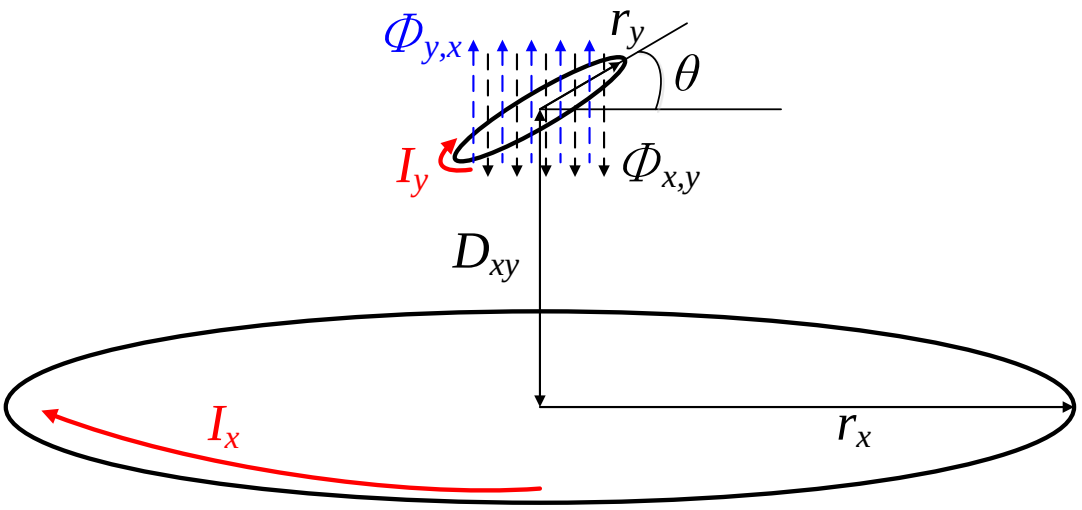

Fig. 2-4. Proposed simple magnetic resonance wireless power transfer coils with geometric and electrical factor for capsule endoscopy.

$$\varepsilon_{y,x} = -\frac{d\Phi_{y,x}}{dt} = -\frac{d}{dt}\int_S \boldsymbol{B}_x \cdot d\boldsymbol{s}_y = -M\frac{dI_x}{dt} \tag{2.9}$$

where is the infinitesimal surface area element defined by the x loop, and M is the mutual inductance between coils.

Combining (2.1), (2.8), and (2.9) creates a new expression in geometric terms (coil radii r_x and r_y, vertical displacement factor D_{xy}, and angle θ) for the coupling coefficient:

$$k_{xy} = \frac{\mu_o \pi r_x^2 r_y^2 \cos\theta}{2\sqrt{L_x L_y}\left(r_x^2 + D_{xy}^2\right)^{3/2}} \tag{2.10}$$

where μ_o is the permeability of the medium, and r_x and r_y are the coil radii. L_x and L_y are the inductances of the coils. D_{xy} is the distance between the coils. This equation indicates that the coupling coefficient could be controlled using vertical displacement factor D_{xy} and angle θ.

2.2.3. Maximum transfer condition

Equation (2.7) expresses the power transfer efficiency of an MR-WPT system. When the relative positions of the TX and RX coils are changed, the modified k_{23} induces a degradation in $|S_{21}|$, which results in a reduced power transfer efficiency for the MR-WPT system. $|S_{21}|$ has a maximum value at the peak value that could be found by the derivative of $|S_{21}|$ with respect to k_{12}. At $d|S_{21}|/dk_{12} = 0$, the maximum efficiency condition of the given MR-WPT system is achieved by the careful control of the k_{12} value:

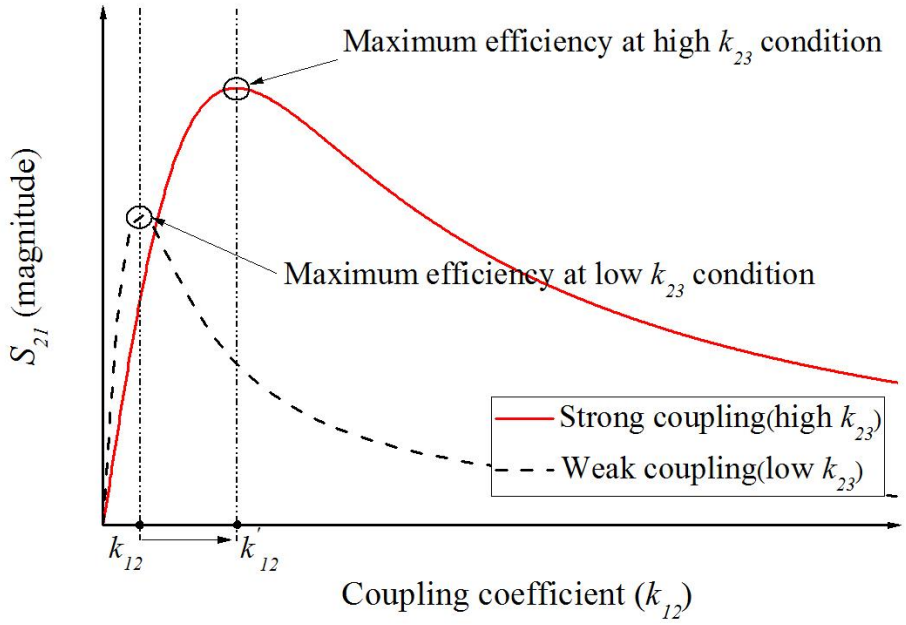

Fig. 2-5. $|S_{21}|$ curves vs. coupling coefficient k_{12}; red line: strong coupling (high k_{23}), black dot: weak coupling (low k_{23}).

$$k_{12} = \sqrt{\frac{R_S R_L R_2 R_3 + R_S R_2 \omega^2 k_{34}^2 L_3 L_4 + R_S R_L \omega^2 k_{23}^2 L_2 L_3}{\omega^4 k_{34}^2 L_1 L_2 L_3 L_4 + R_L R_3 \omega^2 L_1 L_2}} \quad , \quad \text{at } d\left|S_{21}\right| / dk_{12} = 0 \tag{11}$$

Figure 2-5 shows an S_{21} graph of (2.7) and the relationship between k_{12} and k_{23}, where k_{12} is the controllable value, and k_{23} is given by the circumstances. To maximize the transfer efficiency, the optimal k_{12} value can be obtained depending on the k_{23} change caused by the movement of the receiver along the GI tract, as illustrated in (2.10). The coupling coefficient (k_{xy}) is a function of the distance and angle. The value of k_{12} can be optimized to achieve the maximum efficiency of the system by changing the vertical displacement (D_{12}) between the power and TX coils, along with angle θ between the power and TX coils. This new derivation for the MR-WPT system promises a strong power transfer system for biomedical capsule endoscopy applications.

2.2.4. System performance simulation

With the circuit model of the MR-WPT system, the optimum value of k_{12} can be calculated for a given k_{23}. Figure 2-6 shows the improved system performance efficiency due to the proposed technique derived from the circuit model. This result is verified with an advanced design system (ADS) and high frequency structure simulator (HFSS), which are appropriate simulation tools for a WPT system around the frequency of interest at 16.47 MHz [2-12]. In the HFSS simulation, the TX coil is a helical structure with a diameter of 8 cm, 10 turns, and a 0.4-mm pitch between lines. The RX coil is a helical structure with a diameter of 10 mm, 10 turns, and a 0.3-mm pitch between lines. Lumped capacitances of 17.5 pF and 75 pF are used for the TX and RX, respectively. Initially, resonant frequency for this research was chosen above 1 GHz for smaller inductor size benefit. Even though the initial system with resonant frequency beyond 1 GHz showed reasonable performance in the S-parameter analysis with network analyzer [2-13, 2-14], it was not suitable for real power transfer required for capsule endoscopy applications. Because power devices operating near 1 GHz is nearly 10 times more costly than devices operating near 30 MHz. Moreover, passive devices that can operate near 1 GHz with 300 W of power have a much larger form factor size than of passive devices near 30 MHz with 300 W of power. Considering the device size and component price, it was considered much more practical to choose a frequency under 30 MHz. Hence, the resonance frequency for the proposed system is 16.47 MHz. This low frequency is chosen near industrial, scientific and medical (ISM) band of 13.567 MHz, which is widely used in WPT technology, and is suitable for transmitting real power up to 300 W. The maximum efficiency is optimized by changing D_{12}, and the coupling coefficient k_{12} is optimized to the most suitable value. The first setting of the k_{12} value is determined at a TX and RX coil distance (D_{23}) of 15 mm. The proposed MR-WPT system efficiency is improved by 0.67 dB at a distance (D_{23}) of 70 mm and resonance frequency of 16.47 MHz, compared to a non-adaptive MR-WPT system.

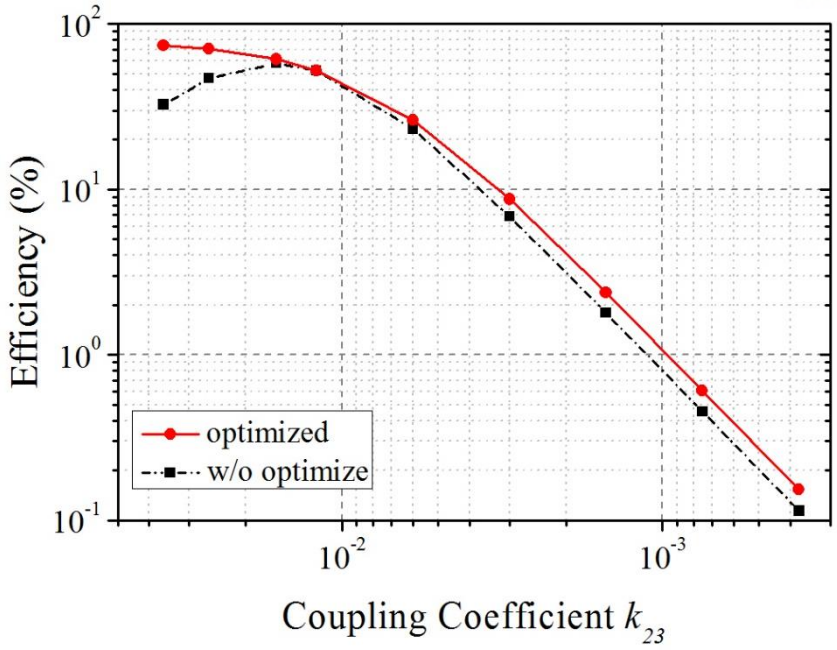

(a)

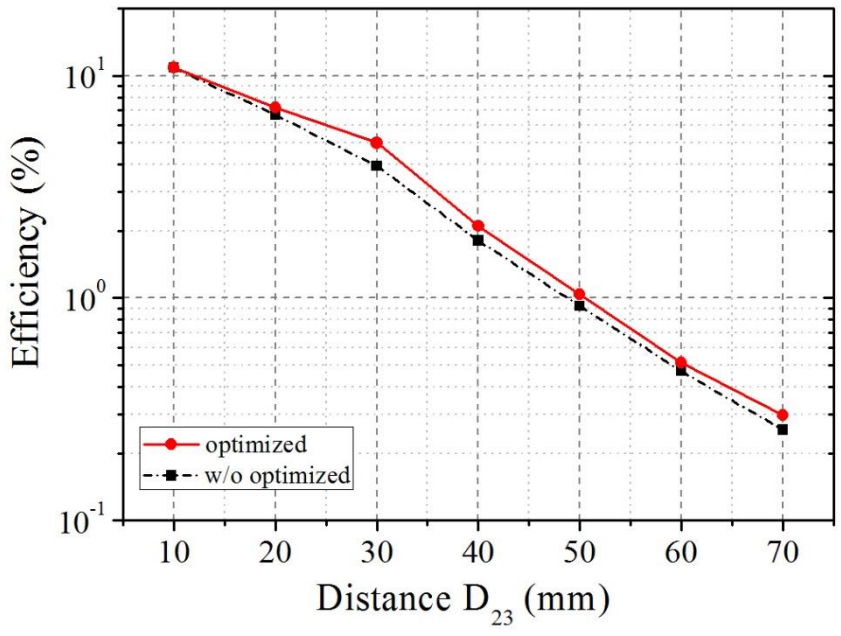

(b)

Fig. 2-6. Performance of self-resonance coupled wireless power transfer system depends on (a) coupling coefficient (k_{23}) varying, and (b) distance between Tx and Rx coils (D_{23}).

2.3. Transmitter and receiver coil structure

The coils are made in the form of magnetic resonance structures. The proposed MR-WPT system consists of four coils: a power coil, transmitter coil, receiver coil, and load coil. The coils are made with copper wires. The cross-sectional diameter of the copper wire is 0.32 mm. Two types of transmitter coil structures are implemented. Both are helical structures, one with an 8-cm diameter and 9.5 turns, and the other with a 22-cm diameter and 6 turns. Both transmitters are designed for the same resonance frequency. In biomedical capsule endoscopy applications, minimizing the RX coil size is always the challenge. This is required because of the very limited volume of the capsule device size. The proposed receiver coil diameter is as small as 9 mm, as illustrated Fig. 2-7. The RX coil also has a helical structure. Because of the stricter coil size requirement compared to that of the transmitter coil, the low-resonance frequency is not easily obtained by the self-resonance frequency of the coil. Thus, a surface-mounted capacitor of 12 pF is used for the receiver coil. This makes it possible to obtain the appropriate resonance frequency in the receiver coil at a sufficiently small form factor. The power coil is slightly smaller than the transmitter coil, with one turn, while the diameter of the load coil is 8 mm. The measured electrical properties of one of the proposed MR-WPT systems with an 8-cm diameter TX coil, a 9-mm diameter RX coil, a TX power coil, and an Rx load coil are summarized in Table 2-2.

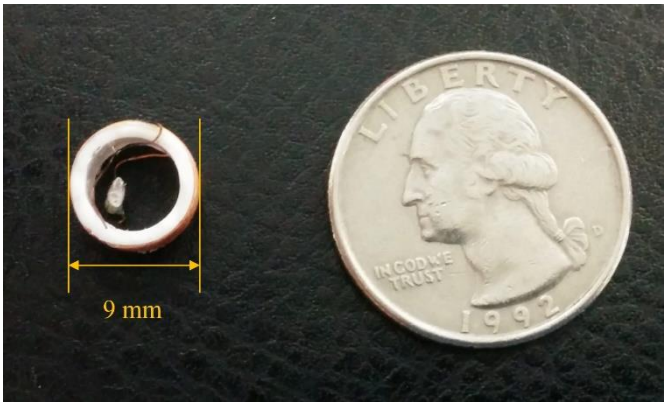

(a)

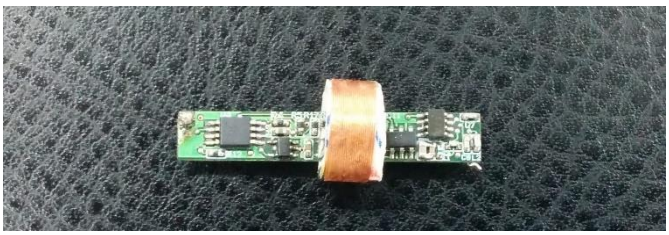

(b)

Fig. 2-7. (a) The designed receiver coil with 9 mm diameter, and (b) Proposed 9-mm WPT receiver paired with capsule endoscopy board.

TX and Power coils			RX and Load coils		
Power coil	C_1	1 nF	Rx coil	C_3	12 pF
	R_1	0.1 Ω		R_3	1.12 Ω
	L_1	221.5 nH		L_3	7.85 µH
Tx coil (8-cm)	C_2	5.48 pF	Load coil	C_4	1 pF
	R_2	0.9 Ω		R_4	0.11 Ω
	L_2	16.14 µH		L_4	30.5 nH

Table 2-2. Measured electrical property of proposed MR-WPT system

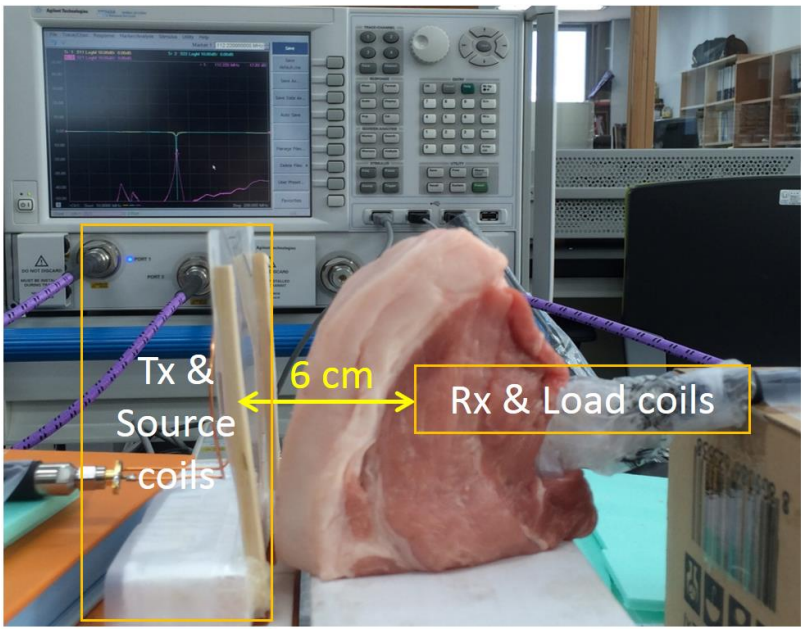

Fig. 2-8. Experimental setup of the impedance mismatched condition.

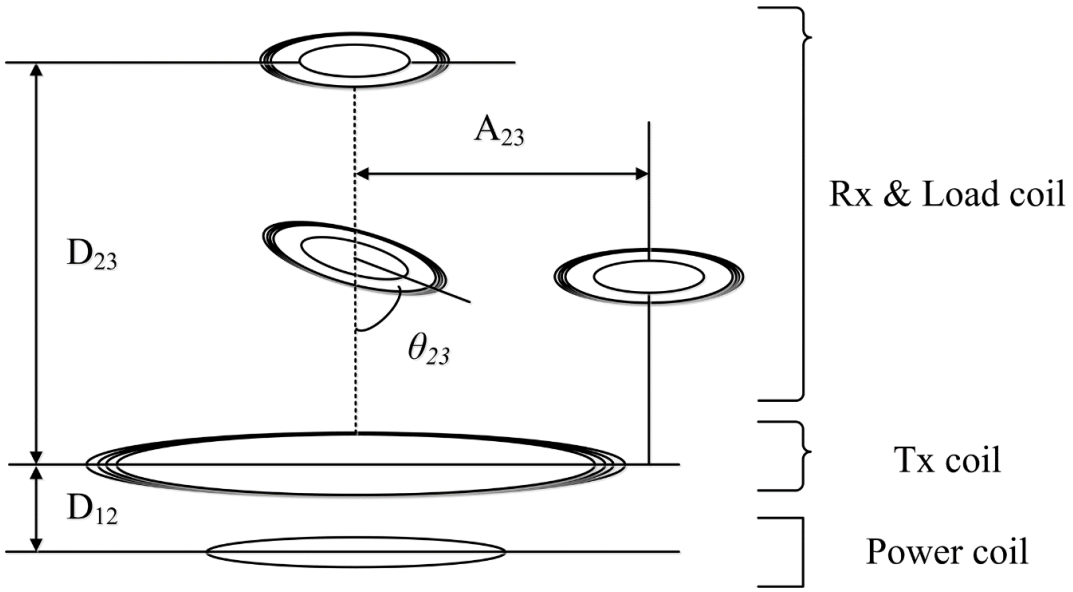

Fig. 2-9. The impedance mismatched condition, (1) between TX and RX coils (D_{23}), (2) angle between TX and RX coil's vertical axis (θ_{23}), and (3) the axial miss-alignment (A_{23}).

2.4. Experimental verification

2.4.1. Experimental setting

In section 2.2, the maximum power transfer condition was analyzed. The proposed method provides a way to track the optimal power transfer condition for the unpredictable movements of the receiver in a patient's GI tract. The coupling coefficient is altered by the distance, axial misalignment, and angle. In this experiment, the proposed method is used for measurements, which are verified over varying values for the distance, axial misalignment, and angle. The measurement setup is shown in Fig. 2-8. The scattering parameter is measured using the PNA-X network analyzer N5242A from Agilent Technologies. Three parameters are shown in Fig. 2-9: the distance between the Tx and Rx coils (D_{23}), angle between the vertical axes of the TX and RX coils (θ_{23}), and axial misalignment (A_{23}). The coupling coefficient of k_{23} is affected by these three parameters. With variable parameters, the coupling coefficient of k_{12} can be optimized using manual control. When the value of D_{23} becomes larger, the value of k_{23} becomes smaller. Under this condition, the optimal efficiency is obtained by increasing D_{12}.

2.4.2. Measured results

First, an actual power transfer to the load coil is demonstrated. The anterior abdominal wall thickness ranges from 3.5 mm to 62.5 mm, with a 16-mm median value. The gastro-intestinal tract is positioned behind a thin part of the anterior abdominal wall, [2-15]. Hence, the distance for the vertical displacement of the proposed system is designed to cover up to 7 cm between the TX and RX coils in order to meet the requirements of conservative cases with an abdominal thickness of 62.5 mm. There is a distance of 7 cm between the human skin surface where the TX coil is located and the RX coil inside the GI tract. The resonance frequency of the TX and RX coils is designed to be 16.47 MHz. An LED is integrated at the end of the load coil. The transmitted power is 158 W, while the received power is measured at 26 mW, as illustrated in Fig. 2-10.

In section 2.2, it was shown that S_{21} is a function of the coupling coefficient k_{12}. The first experiment was performed by varying D_{23}. The S_{21} data were measured while D_{23} was varied from 10 to 100 mm, as illustrated in Fig. 2-9. The overall efficiency was degraded with an increase in D_{23}. The first optimized point was set at 10 mm. After a change in D_{23}, the optimum D_{12} was applied. Thus, the optimized point was found, as shown in Fig. 2-10(a). The improvement in efficiency was increased from 27.79 to 32.43% (0.67 dB) at 20 mm. The improvement in efficiency was increased from 9.4×10^{-2} to 1.65×10^{-1}% (2.45 dB) at 100 mm. This experimental result is in agreement with the simulation result illustrated in Fig. 2-6.

In Fig. 2-10(b), the measured S_{21} data with θ_{23} varied from -90° to 90° at a distance of 70 mm are demonstrated. The varied D_{12} was applied to track the optimal transfer efficiency. The improvement in efficiency was increased from 0.55 to 0.71% (1.1 dB) at -15°. The improvement in efficiency was increased from 3.6×10^{-3} to 8.1×10^{-3}% (4.69 dB) at -90°.

In Fig. 10(c), the measured S_{21} data with the axial misalignment A_{23} varied from -50 mm to +50 mm at a 70-mm vertical displacement (D_{23}) are demonstrated. The improvement in efficiency was increased from 6.5 × 10^{-1} to 7.1 × 10^{-1}% (0.49 dB) at 10-mm. The improvement in efficiency was increased from 5.2 × 10^{-2} to 7.3 × 10^{-2}% (1.48 dB) at -50-mm axial misalignment.

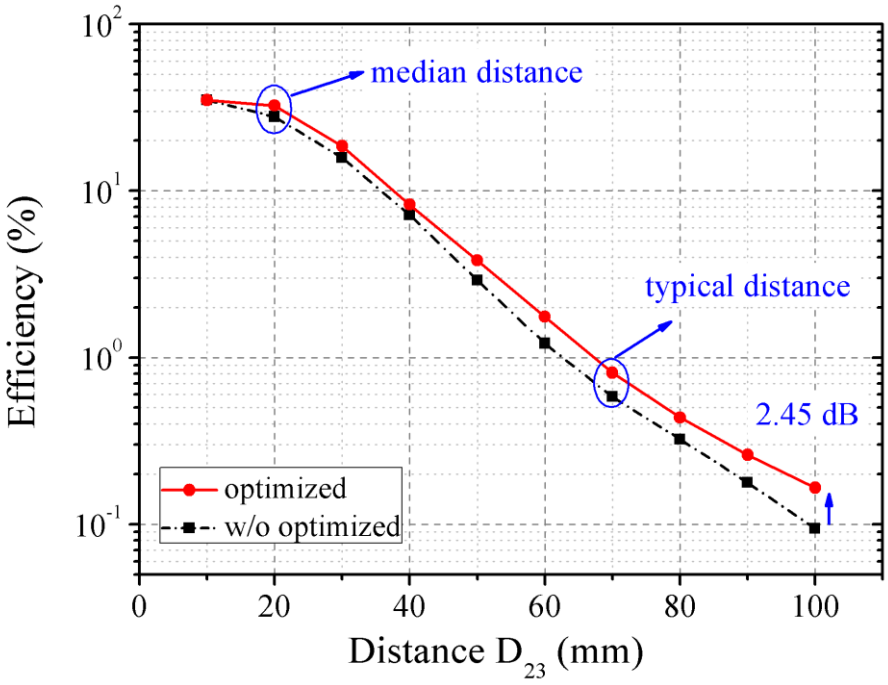

(a)

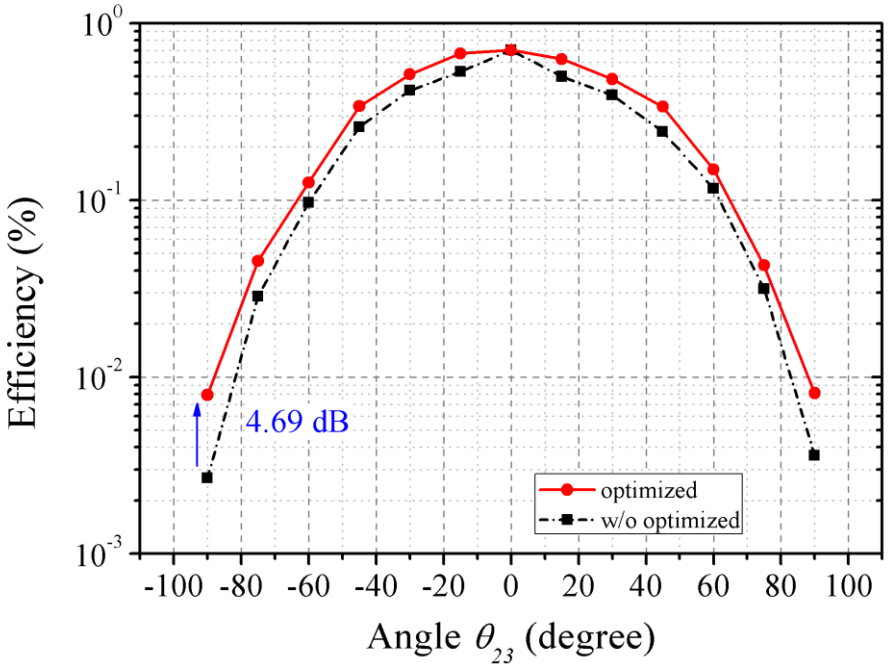

(b)

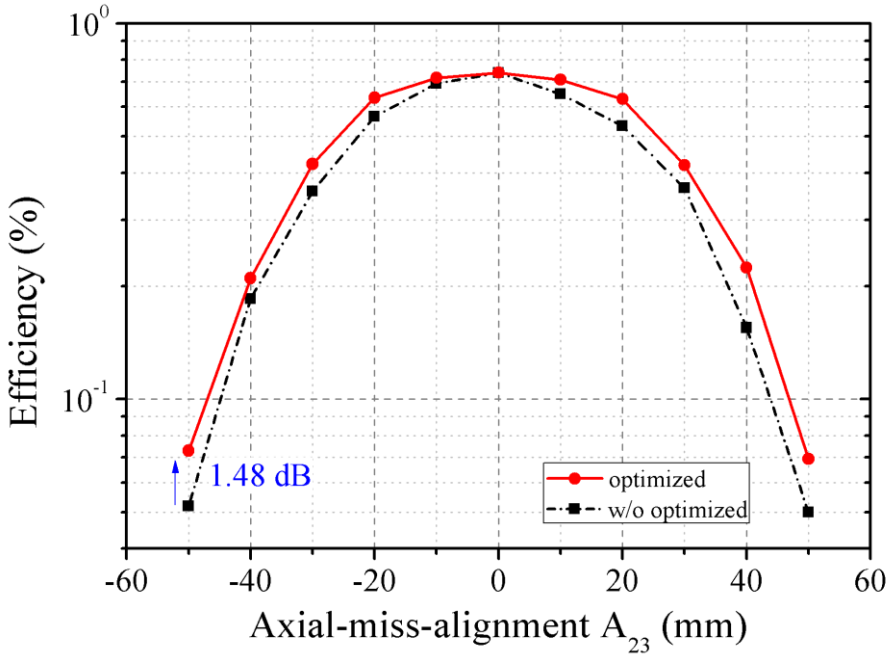

(c)

Fig. 2-10. Measured performance of the proposed work: (a) D_{23} VS. S_{21} graph w/o optimize and w/ optimize. (b) θ_{23} VS. S_{21} graph w/o optimize and w/ optimize. (c) A_{23} VS. S_{21} graph w/o optimize and w/ optimize of resonance coupled wireless power transfer system.

2.5. Safety issue on wireless power transfer

When human is exposed to electromagnetic waves, temperature of the tissue is increase by absorbed energy. This elevate tissue temperatures and increases risk of cancer. Thus, Safety verification test required. In this chapter, it is verified that the wireless power transmission is able to transmit power through the real tissue. Verification test that the wireless power transmission is harmless or harmful to the human body is performed.

2.5.1. Penetration experimental though real tissue

During the research on the MR-WPT system for biomedical applications, there were many issues regarding the transfer efficiency through real tissue. Based on the electromagnetic theory, a time-variant magnetic flux can induce a current through a conducting material. The conductivity of real tissue is negligible compared to metal, and hence should not affect the transfer efficiency. Fig. 2-11 shows the human body channel model developed for a frequency range of 40 Hz to 110 MHz [2-16], along with the simulation results using this model. The results show a 0.394-dB difference at the maximum point, which is equivalent to a 6.4 $\times$ 10^{-2}% decrease. Fig. 2-12 illustrates the experimental setup to determine the penetration through biological tissue using a pork chop. The distance between the TX and Rx coils was 7 cm. The RX coil was deep inside the pork chop, and there was no path without going through the pork tissue.

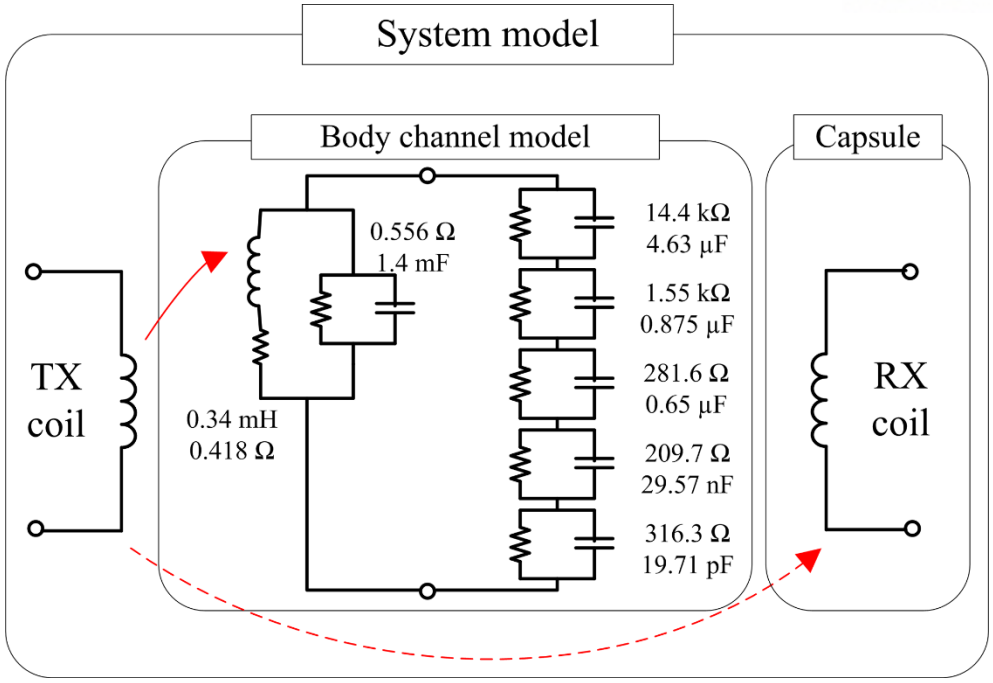

(a)

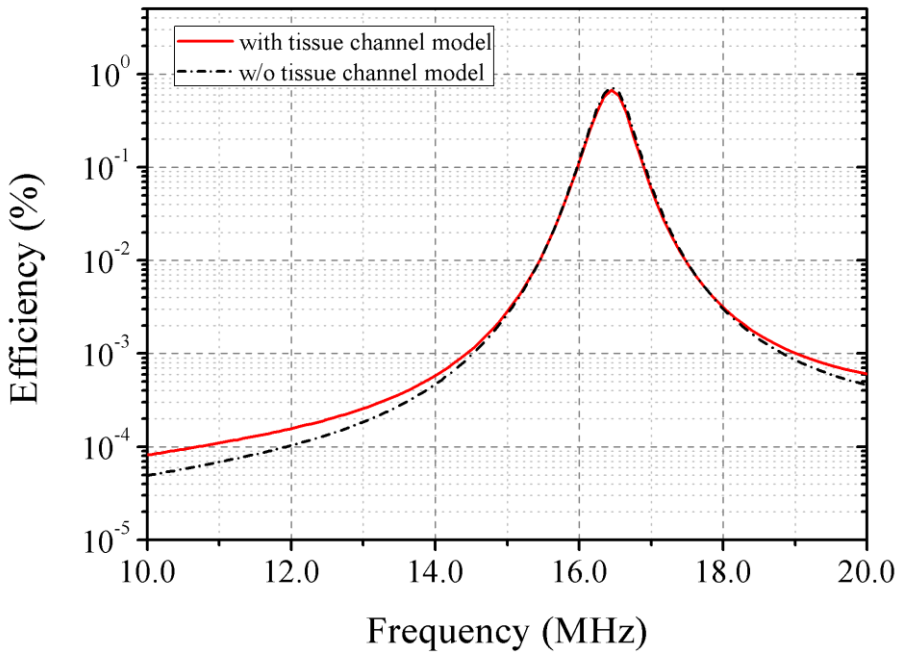

(b)

Fig. 2-11. (a) Human body channel model, and (b) simulation result

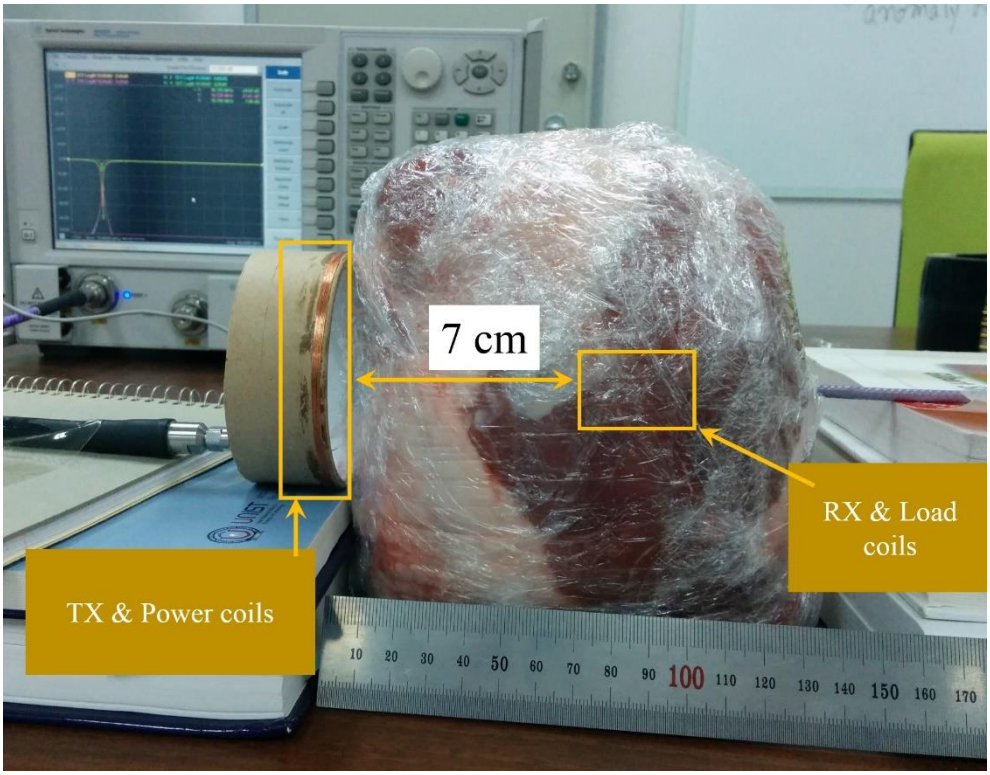

Fig. 2-12. Penetration experiment setting with pork chop

Figure 2-13 shows the measured efficiency result of the penetration experiment through the pork chop at the same distance, angle, and axis-alignment. As shown in Fig. 2-13, the maximum transfer efficiency was almost the same; it had only a 0.390-dB difference, which was equivalent to a 6.2×10^{-2}% decrease. This experimental result is consistent with the channel model simulation result.

In order to further demonstrate the safety to the human body, thermogram images were taken to check the energy loss dissipated as heat. Fig. 2-14 shows the monitored temperature change in the biological tissue for the worst-case scenario, which was measured with a 22-cm diameter TX. After a power transmission for 1 h at a distance of 0 cm, there was no change in the temperature of the biological tissue, which was well below the 1.0°C safety guideline. These results show the possibility of using the proposed MR-WPT system for biomedical applications.

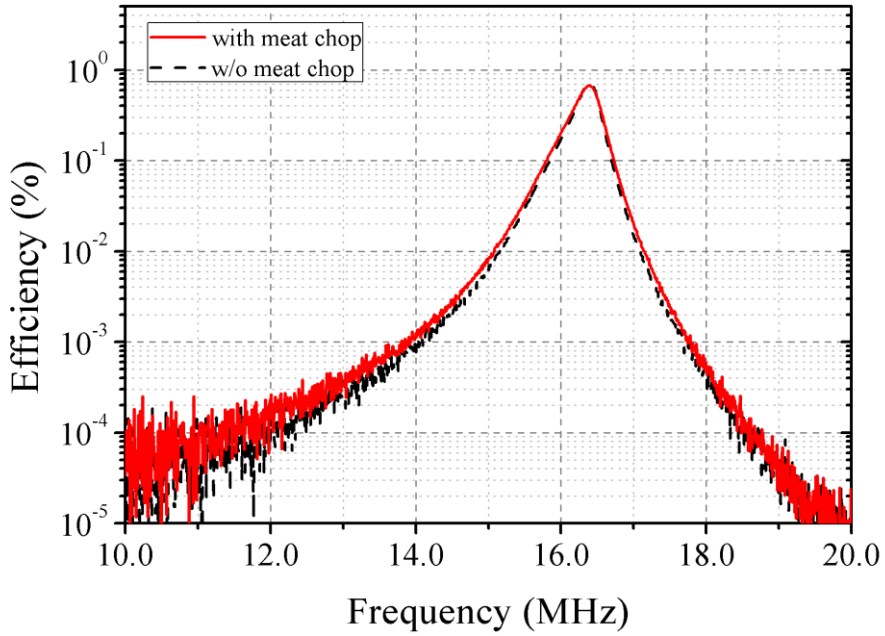

Fig. 2-13. Measurement result of penetration experiment through real biological tissue at 7-cm distance.

(a)

(b)

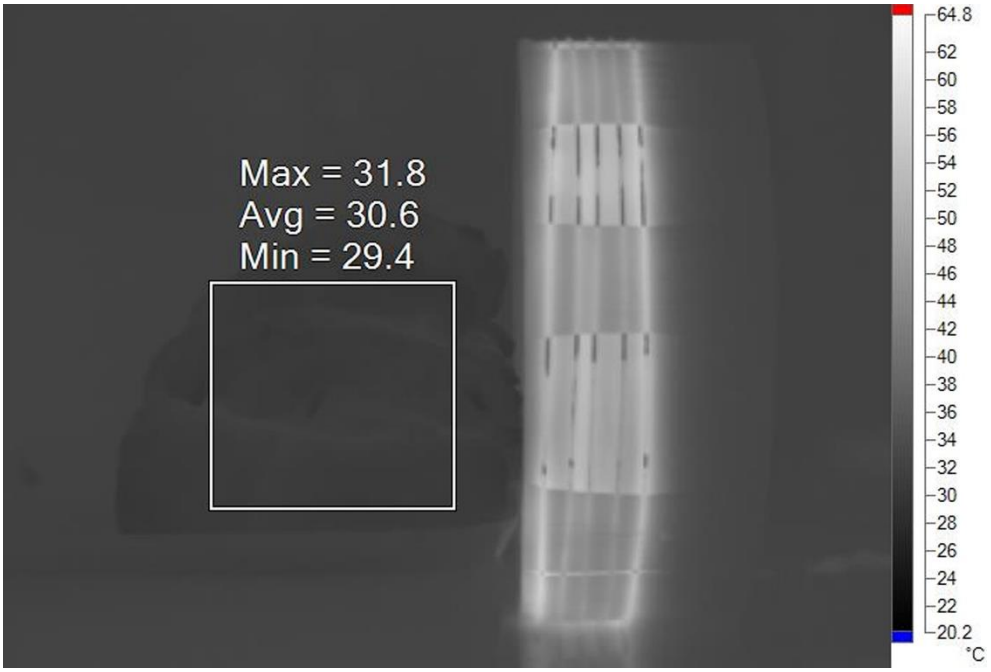

(c)

Fig. 2-14. Thermogram of 22-cm diameter TX with 7-cm distance to biological tissue (a) visible light image, (b) before power transmission, and (c) after 1-hour power transmission.

Classification		Korea	Japan	USA	CENELEC	ICNIRP	IEEE
Frequency range		100kHz~ 10GHz	100kHz ~3GHz	100kHz~ 600MHz	10kHz~ 300GHz	100kHz~ 10GHz	100kHz ~3GHz
Normal man (W/kg)	Whole body	0.08	0.08	0.08	0.08	0.08	0.08
	Head/Trunk	1.6	2	1.6	2	2	2
	Arm/Leg	4	4	4	4	4	4
Career man (W/kg)	Whole body	0.4	0.4	0.4	0.4	0.4	0.4
	Head/Trunk	8	10	8	10	10	10
	Arm/Leg	20	20	20	20	20	20

Table 2-3. Specific absorption rate regulation in countries and international organization.

2.5.2. Specific absorption rate (SAR)

For biomedical applications of electro-magnetic (EM) field-generating devices, the EM field absorption in the body has to be satisfied. The SAR is a measure of the rate at which energy is absorbed by the human body, defined as W/kg. If the SAR becomes too high, it can cause harm to the human body. At a frequency range of 1 Hz to 10 kHz, the EM field stimulates the nerve cells. At a frequency range of 100 kHz to 10 GHz, the absorbed EM energy causes a temperature increase in a human.

Thus, many countries and organizations set restrictions of 0.08 W/kg to the whole body, 1.6 or 2 W/kg to the head/trunk, and 4 W/kg to the arm/leg at a frequency range of 100 kHz to 300 GHz. SAR regulation guides is shown in Table 2-3. If the whole human body is exposed to a strong EM field, the temperature increase becomes more severe. Thus, the restriction is stricter than the partial absorption rate [1-6 ,2-17~19].

Therefore, the SAR was estimated for the proposed MR-WPT system using the HFSS simulation tool. The human body was modeled with water. Fig. 2-15 shows the 3-D graph produced using the SAR analysis results, where Fig. 2-15(a) indicates the positioning of the TX coils and RX coils. The RX and load coils are cylindrical shape capsule models, which are covered by water. In the SAR analysis, the efficiency of the system was 0.2% (-27 dB) at a 7.3-cm distance. The transmitting power from the TX was 150 W, and 300 mW of energy was received at the load coil. The maximum SAR value was very small at 1.74 W/kg. A smaller amount of energy compared with the restriction was absorbed in a limited area of the human body. Thus, the safety of the proposed MR-WPT system in the human body was confirmed.

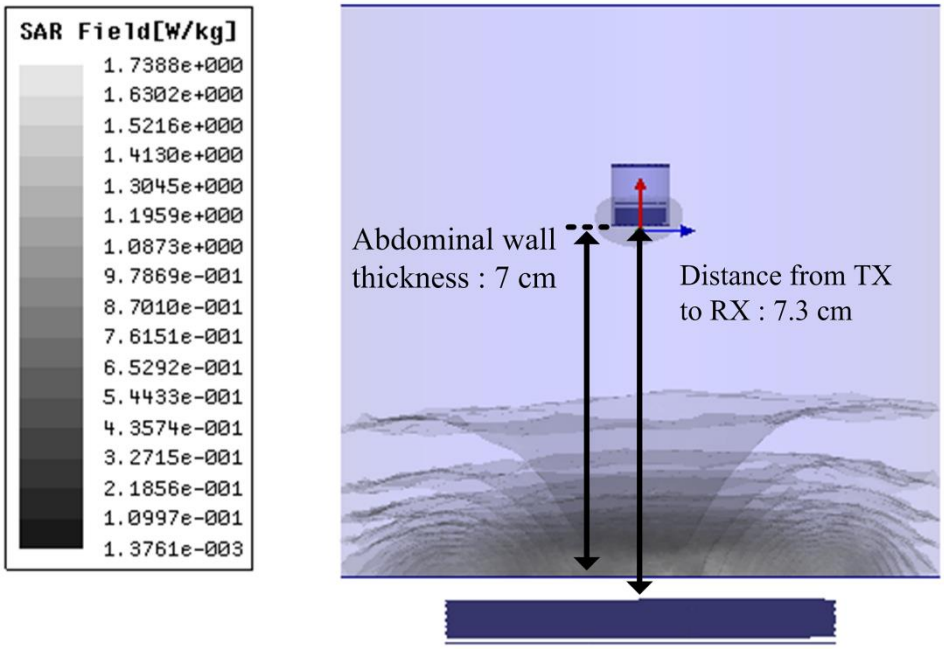

(a)

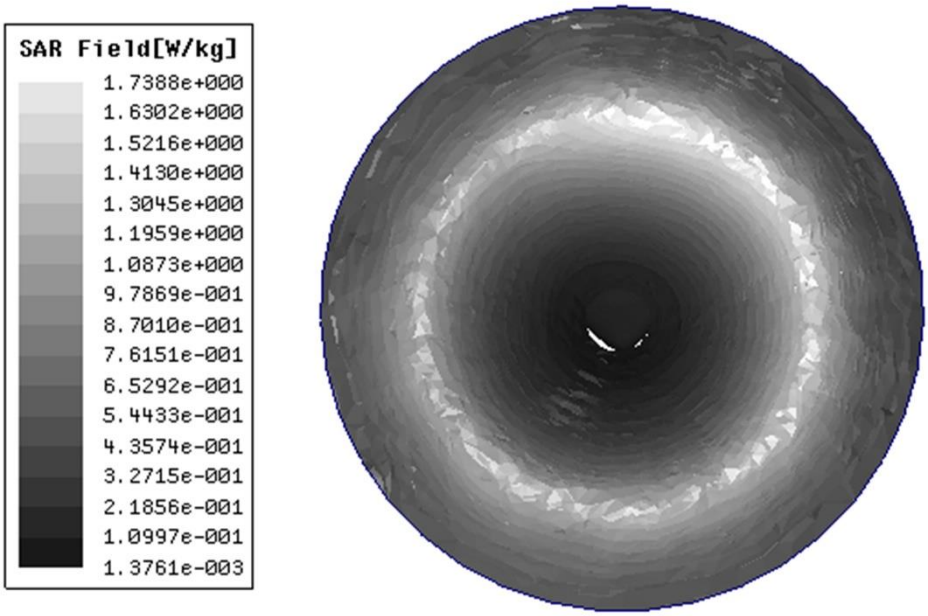

(b)

Fig. 2-15. 3-D graph of specific absorption rate (SAR) for the proposed MR-WPT system (a) side view; and (b) bottom view.

2.6. Summary

In this chapter, a new method to track the maximum efficiency of an MR-WPT system suitable for biomedical capsule endoscopy application was presented. The theoretical proof was followed by the results of simulations and measurement experiments. Since capsule endoscopy require a small form factor, a 9-mm diameter receiver with a 16.47-MHz resonance frequency was designed, and the performance was measured. In order to track the efficiency while the receiver was in the GI tract with variations in the distance, angle, and axial-misalignment to the transmitter, a new adaptive method was proposed. This adaptive technique utilizes the coupling coefficient k_{12}. In the distance change situation (D_{23} between the Tx and Rx coils), the efficiency was increased by up to 2.45 dB with the proposed work. In the angle change situation (θ_{23} between Tx and Rx coils), the efficiency is increased up to 4.69 dB. In the axial misalignment case, (A_{23} between Tx and Rx coils), the efficiency was increased by up to 1.48 dB. It was demonstrated experimentally that the proposed MR-WPT system for capsule endoscopy applications is able to track the optimal efficiency under various geometric factors while transferring a real power of 26 mW to the load at a distance of 7 cm.

Because the proposed work is intended for biomedical application, penetration experiments through real biological tissue were performed. There was minimal effect on the efficiency when the receiver and load coils were tested inside a tissue block at a depth of 7 cm, with a degradation of only 0.39 dB. The SAR test showed a very low value of 1.74 W/kg, with an energy transfer condition of 300 mW to the load. This confirmed the safety of the proposed MR-WPT system for use in a human body.

Chapter III

Power control technique for variable load of battery in wireless power transfer system.

3.1. Background

A cardiac pacemaker is a medical device which uses electrical impulses to contract the heart muscles, to regulate the beating of the heart for people having heart disease. Since heart failure does not know when to come, patients have a pacemaker on their chest to cope with the sudden danger is implanted. Although the pacemaker is a device that alleviates the patient's life, it is also a device that causes great discomfort at the same time. The length and height of the pacemaker are around 50 mm and 40 mm. The thickness of the device is around 6 mm. The real image of pacemaker is shown in Fig. 3-1. Devices such as pacemakers are much larger than other biomedical devices, and as you can see in the picture, about 50% of the inside is a battery. Furthermore, as mentioned in Chapter I, it is necessary to replace the battery every 8 to 10 years to remove the battery [1-5]. WPT technology is required to solve this problem. Prior to discussing which WPT technology to use, it is necessary to know where the device is being implanted in order to determine the appropriate WPT for this device. Fig. 3-2 shows X-ray image of the human body with implanted pacemaker. The pacemaker is mounted on the left chest or the left waist and is mounted directly under the skin of the chest and the waist. It is not a device that keeps moving like a capsule endoscopy. Therefore, IPT technology is suitable technology for devices such as pacemaker. Although the efficiency distance is shorter than that of MR-WPT, it is very efficient in short-distance transmission. Although IPT technology is highly efficient, the power stage for battery charging is increased, which eventually becomes a loss, causing the temperature of the device to rise during charging. Therefore, there is a need for a method that can further increase the efficiency. “Step charging method” for IPT using in-band communication is proposed for charging without a additional battery charger. Fig. 3-3 shows the proposed system block diagram for power control technique for variable load. This consists of primary side and secondary side circuits. Main power stage of this system is half-bridge inverter, primary side coil, secondary side coil and rectifier. Power is controlled by frequency modulation. MCU and in-band communication is used for PWM controller and feedback control.

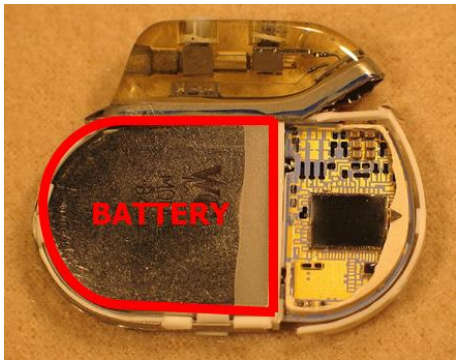

Fig. 3-1. Inside of the cardiac pacemaker.

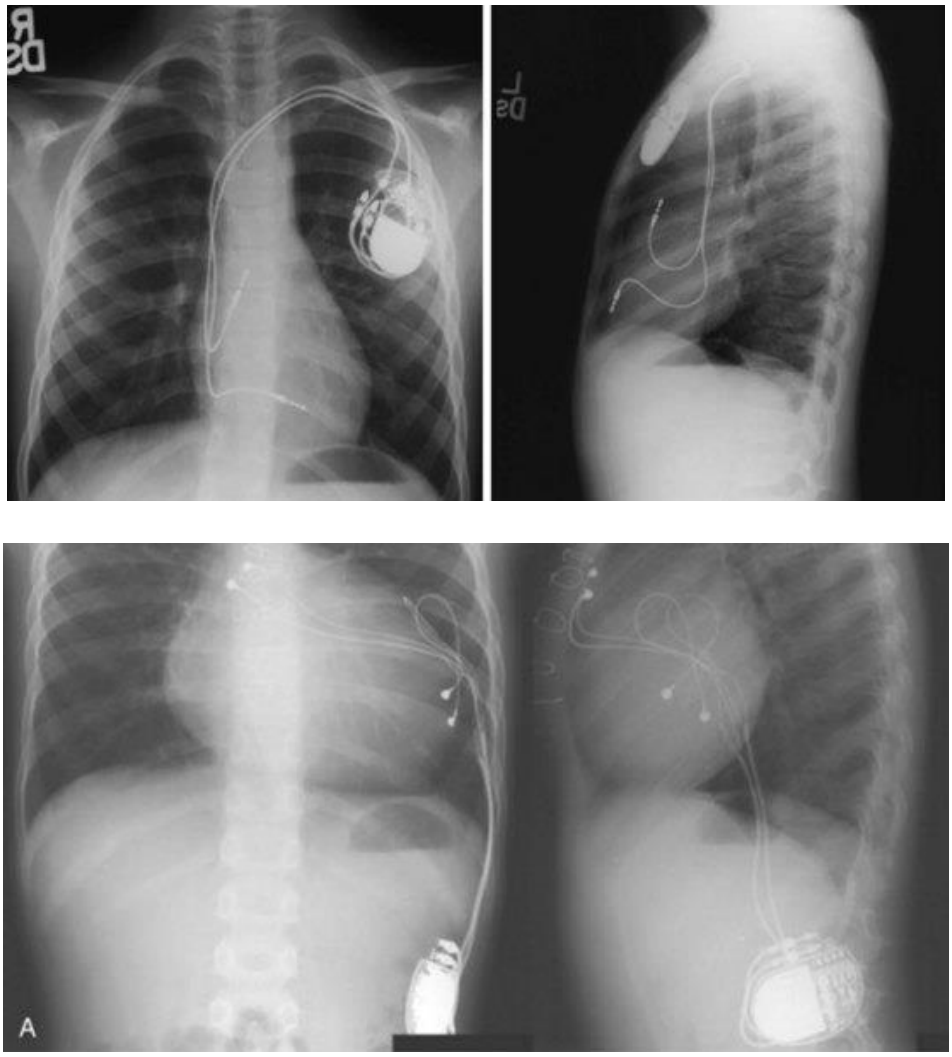

Fig. 3-2. X-ray image of human with implanted pacemaker.

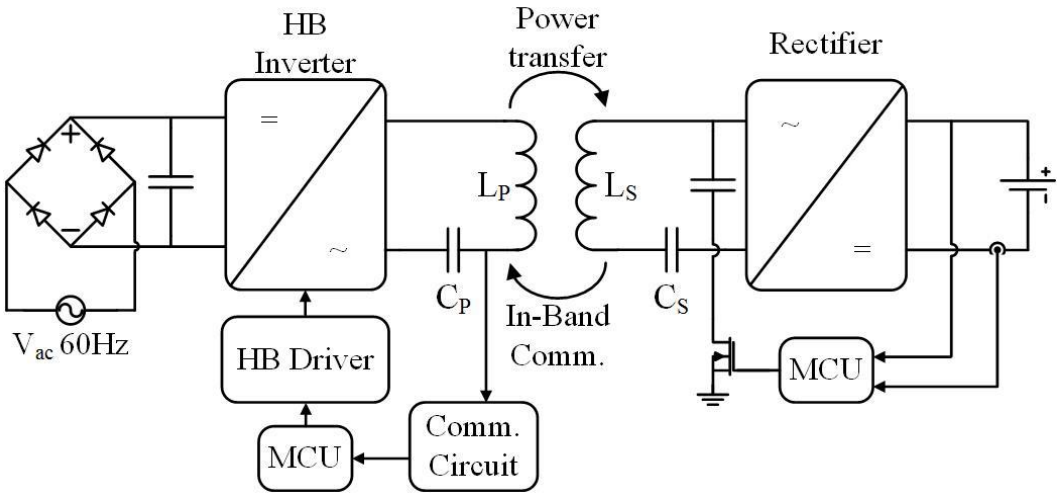

Fig. 3-3. Proposed IPT block diagram with battery charger in receiver.

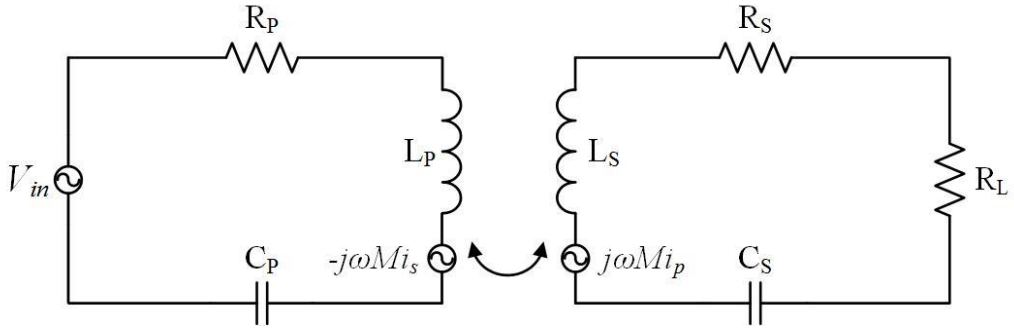

Fig. 3-4. Equivalent circuit of series-series compensated IPT.

3.2. Frequency modulation technique analysis

Prior to the newly proposed charging method, the power control method of the frequency modulation (FM) method which is the basis of the charging method is analyzed. For IPT hardware to demonstrate the proposed power control technique, SS compensation is used because of its simple structure and the voltage step-down characteristics compared to the SP, PS and PP compensation topologies. An equivalent circuit of the SS compensated IPT system is shown in Fig. 3-4. The circuit can be used to obtain load current of the network with respect to switching frequency f. The impedance of primary side is

$$Z_p = j\omega L_p + \frac{1}{j\omega C_p} + R_p \tag{3.1}$$

And the impedance of the secondary side is

$$Z_s = j\omega L_s + \frac{1}{j\omega C_s} + R_s + R_L \tag{3.2}$$

where R_x is the resistance, L_x is the inductance, and C_x is the capacitance, with subscript "P" for the primary side and "S" for the secondary side. Also, R_L is the equivalent resistance of the battery load and ω is the angular frequency $2\pi f$. The voltage gain of the circuit is expressed as

$$G_V = \frac{V_{out}}{V_{in}} = \frac{\omega M}{Z_p Z_s + \omega^2 M^2} R_L \tag{3.3}$$

where V_{in} is input voltage at the primary side, V_{out} is the output voltage at the secondary side, and M is the mutual inductance of L_p and L_s. Since there is a rectifier with a capacitor filter, which acts as an impedance transformer, R_L can be modified as an equivalent ac resistance [3-1~3]. The load resistance of R_L can be replaced by $R_{L\text{-}AC}$, which is expressed according to the battery voltage V_{batt} and the charge current I_{char} as

$$R_{L-AC} = \frac{8}{\pi^2} \frac{V_{batt}}{I_{char}} \tag{3.4}$$

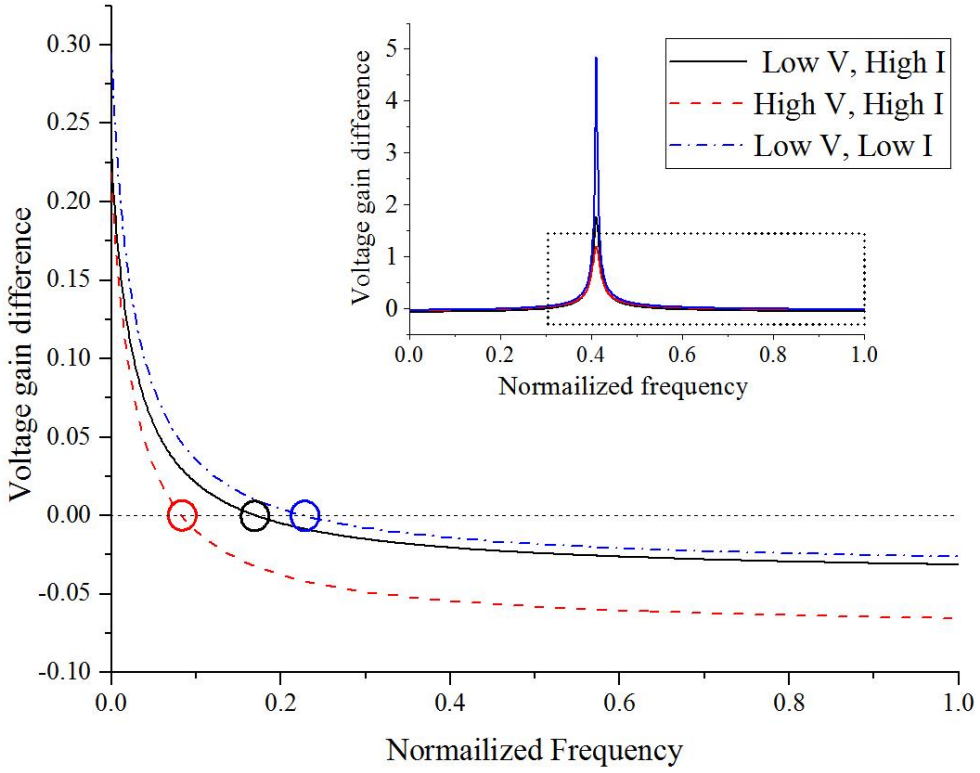

Fig. 3-5. Voltage gain difference graph according to the normalized frequency at different voltage and current conditions

According to (3.3) and (3.4), frequency could be controlled to supply constant current on the battery. Mutual inductance and voltage is given by the position of the coils and battery characteristics. The charging current is predetermined based on the recommended charge current rating for the battery. The optimal frequency can be derived from the following:

$$G_{v-diff} = G_{v-freq} - G_{v-voltage} = V_{batt}\left\{\left|\frac{8\omega M}{\pi^2(Z_pZ_s+\omega^2M^2)I_{char}}\right| - \frac{1}{V_{in}}\right\} \quad (3.5)$$

where G_{v-diff} is the voltage gain difference between the gain according to the frequency (G_{v-freq}) and the desired gain ($G_{v-voltage}$). At the $G_{v-diff} = 0$ condition, when the gain of the frequency matches the desired gain, we can find the control frequency for the desired current and voltage. Fig. 3-5 shows G_{v-diff} according to the normalized frequency.

The frequency needs to be close to the resonance frequency when the charging current or battery voltage are increased. The frequency below the resonance frequency is the capacitive region, where current leads. In this region, shoot-through current at half-bridge inverter switch diode can occur [3-4]. Because of this, the region above the resonance frequency is used for adaptive frequency modulation. Fig.3-6 shows charging frequency with respect to the battery voltage. Battery charging voltage and current are adjustable via FM. The calculated frequency is extracted from (3.5), assuming input voltage is fixed and the battery charging current is 4 A. The calculated results are well-matched to measured results, with a maximum 1 kHz difference between the measured and calculated frequency, which is only 0.7% error. This discrepancy is caused by nonidealities in the real circuit containing a half-bridge inverter and other components, which are neglected in the ideal circuit shown in Fig. 3-4.

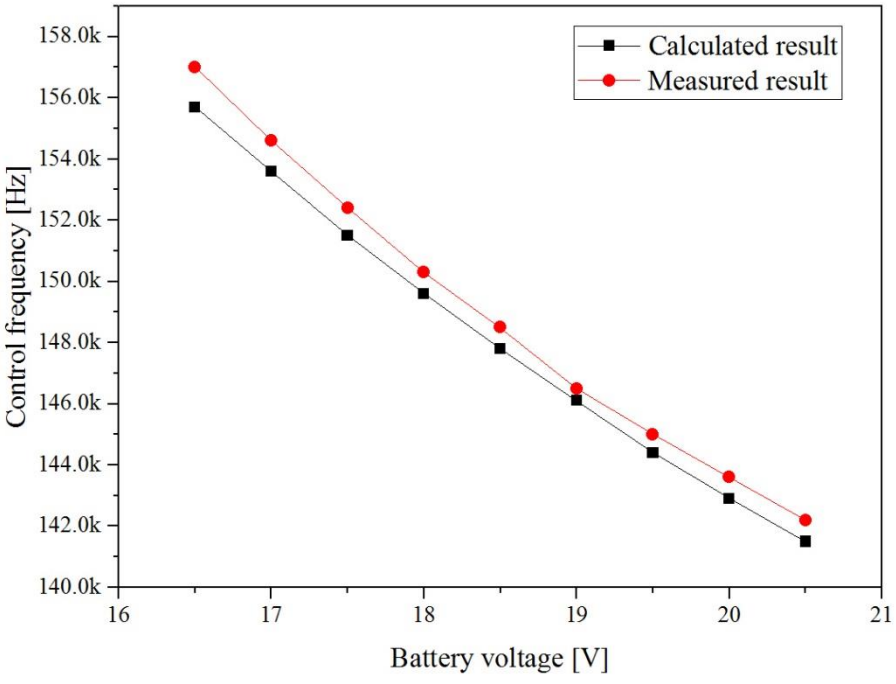

Fig. 3-6. Charging frequency according to the battery voltage at fixed charging current condition.

3.3. Proposed step charging method

3.3.1. Battery characteristic

Before dealing with battery charging technology, the battery characteristics must be known. As mentioned in chapter I, all rechargeable batteries be charged in CC/CV mode. CC mode is related to battery life and CV mode is related to battery safety. Constant current minimizes battery life degradation. And if the battery voltage exceeds the allowable value, the battery explosion or life time is greatly shortened. The proposed technology satisfies this CC/CV mode conditions when charging battery with extra battery charger. This charging method uses battery hysteresis features. Fig. 3-7 shows the voltage hysteresis of the rechargeable battery. Batterie of the same capacity has different voltages when charging and discharging. This voltage difference is called voltage hysteresis. The reason for this phenomenon is known to be due to chemical changes in the battery, but it is not yet clearly discovered. Fig. 3-8 shows difference of the voltage hysteresis depending on amount of the charging and discharging current. When the charging and discharging current is 1A, voltage hysteresis can be expressed as V_{H1}. When charging and discharging current is 2A, voltage hysteresis can be expressed as V_{H2}. As shown in the figure above, voltage hysteresis is a value having different values depending on the amount of current. In order to charge the battery, it is necessary to know the above characteristics. In this study, the battery charging technique using voltage hysteresis is proposed.

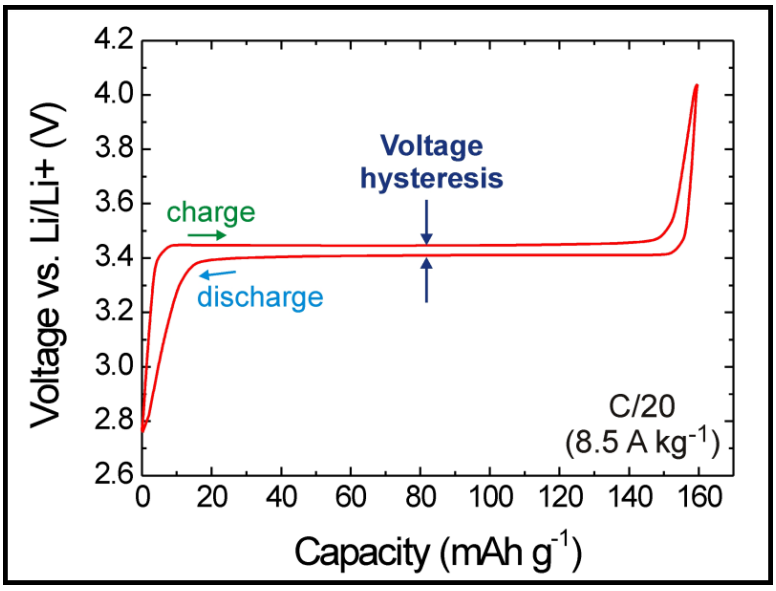

Fig. 3-7. Voltage hysteresis of rechargeable battery [3-5].

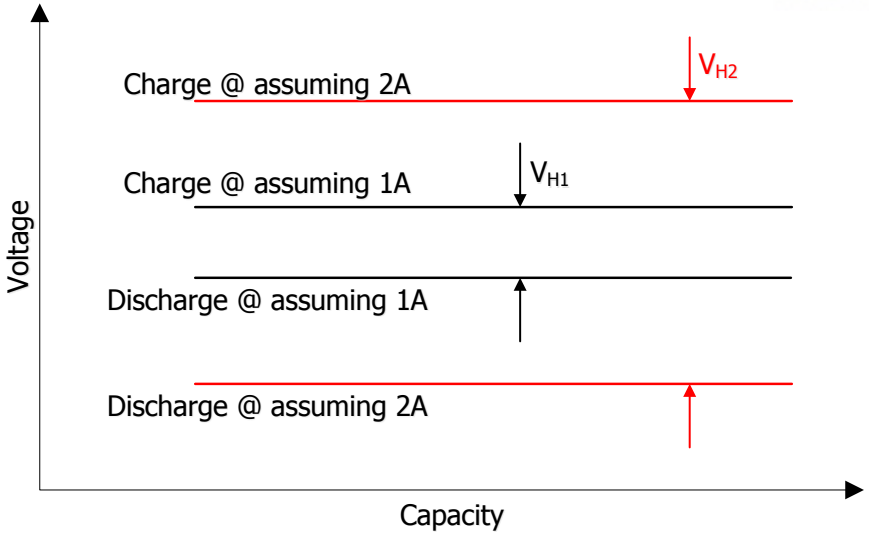

Fig. 3-8. Voltage hysteresis depending on amount of current.

3.3.2. Algorithm

The proposed step charging method using FM can enhance the power transfer efficiency with minimized power stages, simple communication system and minimized feedback control. To implement this technique, operations of the primary and secondary sides have to be connected by the algorithm through one-way communication from the secondary to primary side. A flow chart of the algorithm is shown in Fig. 3-9, outlining the procedure for CC and CV mode battery charging. This algorithm is implemented on a frequency controllable IPT system using in-band communication.

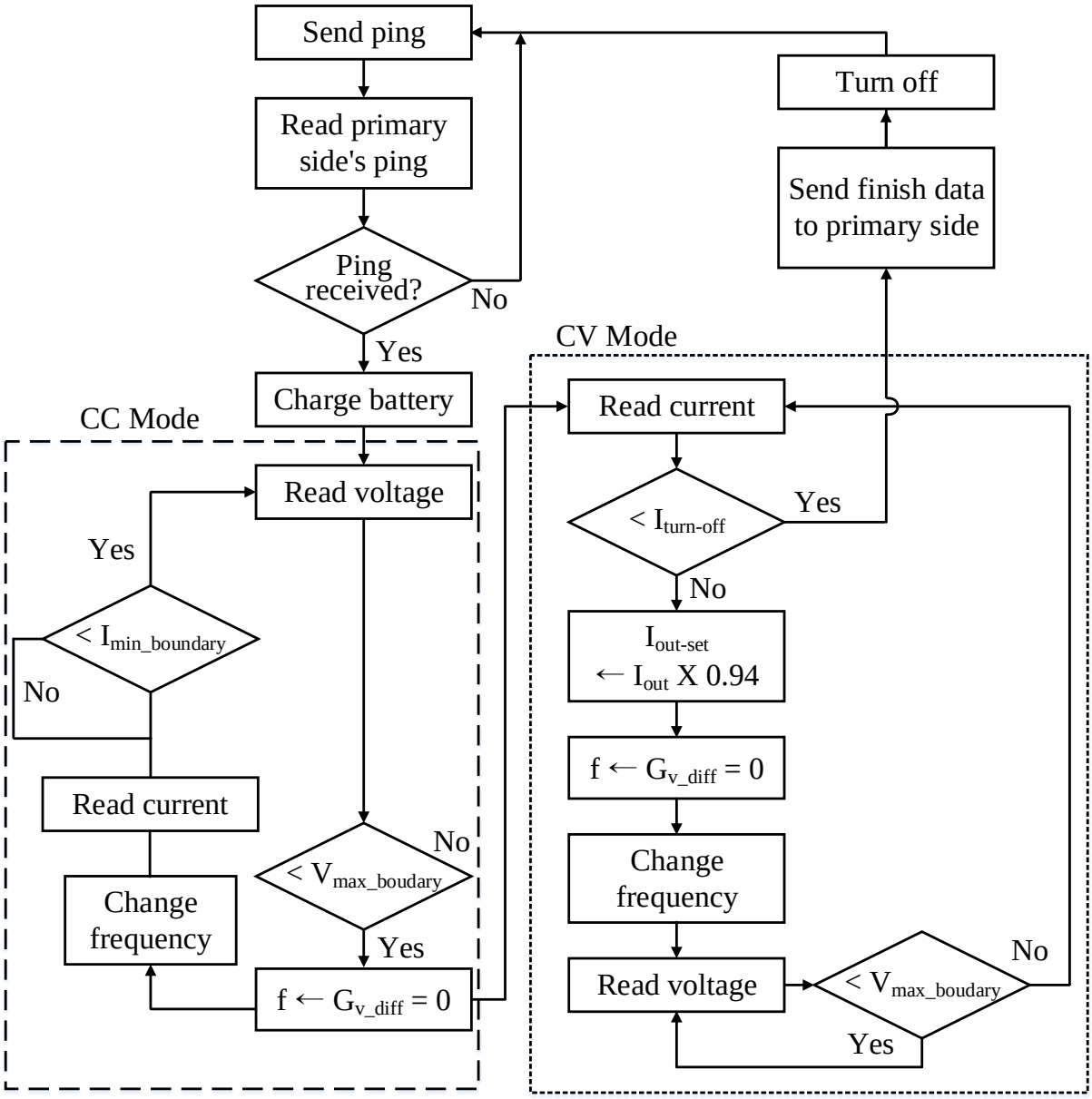

Fig. 3-9. Flow chart of the proposed adaptive frequency modulation for battery charging system.

Before charging the battery, the primary side sends a ping repeatedly to check if the secondary side coil is properly placed for charging. The primary side can detect the secondary side itself without communication. If a battery is recognized, the primary side starts the charging process. Then, the system checks the battery voltage and sends the calculated frequency data based on (3.5). After this data transfer, the primary side begins charging at the given frequency to charge the battery on the secondary side around the current given by the battery profile.

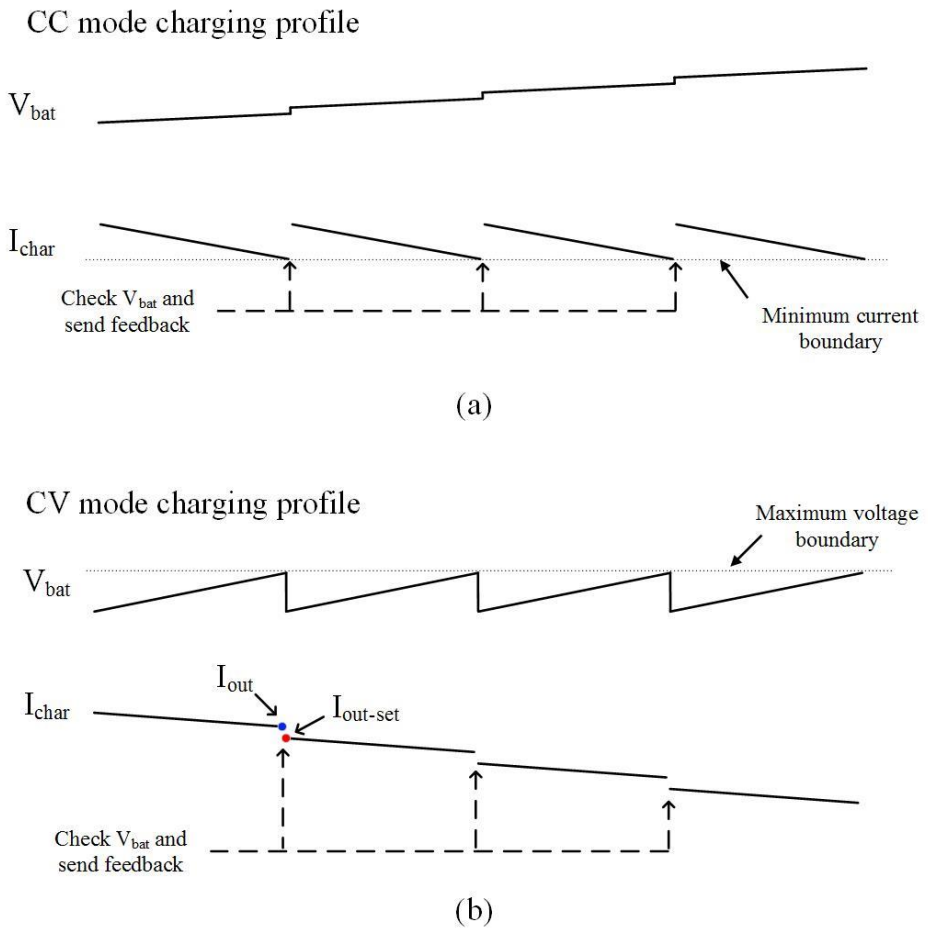

Fig. 3-10. Proposed step charging method in frequency controllable IPT using in-band communication. (a) CC mode. (b) CV mode.

In CC mode, the secondary side reads the battery voltage when charging current I_{char} reaches the minimum current value $I_{\text{min\_bodundary}}$, which is selected after considering the frequency resolution of the MCU, and sends feedback data to the primary side to maintain the average current at the current given by the battery profile. This sequence is illustrated in Fig.3-10(a). This sequence is continued until the battery voltage reaches $V_{\text{max\_bodundary}}$, which is fully-charged battery voltage given by the battery profile.

In CV mode, the charge current should decrease over time according to the battery conditions. To realize CV

mode with an MCU, which control frequency discretely, a current step charging method is applied, which is shown in Fig. 3-10(b). The battery exhibits hysteresis, shown as a drop of battery voltage proportional to the charging current. The current step charging method uses the battery hysteresis. In the flow chart, the previous charging current is expressed as I_{out} and the next target charging current is expressed as $I_{out-set}$, which is set to $I_{\text{out}}\times 0.94$. When the battery voltage reaches the maximum acceptable voltage, which is $V_{\text{max\_bodundary}}$ in the target application, the secondary side sends the new frequency data to the primary side to reduce the charging current to $I_{out-set}$. With the reduced charging current, the charging voltage is decreased below $V_{\text{max\_bodundary}}$. Since the battery has the voltage hysteresis of battery, when the battery voltage reaches the maximum value, when charging current is reduced, the charging voltage can be lowered, so that the battery can be charged without overvoltage charging. This sequence continues until the battery charging current reaches the minimum charging current, which is $I_{turn-off}$ for the target application. By using this algorithm, the battery can be charged in CC/CV mode condition without a regulator/

In addition to the charging procedure, protection is included in the proposed charging algorithm. The implemented protection programs are over-voltage protection, over-current protection, and temperature protection. For over-voltage and over-current conditions, the charging system shuts off completely. For high temperature conditions, the charging current is reduced for 10 minutes to limit the heat generation.

3.4. System description

In this section, system hardware used to validate the IPT for battery charging is described. The primary side (power transmitter) and secondary side (power receiver) circuits are described. And The characteristic of primary and secondary side coils for frequency modulation is described. The communication circuit used for sending feedback data about frequency over voltage, current and temperature from the secondary to primary side is described.

3.4.1. Transmitter and receiver circuits

The primary side schematic is shown in Fig. 3-11. The hardware of the primary-side board is shown in Fig. 3-12(a). The system parameter and components used in the circuit are summarized in Table 3-1. In input voltage is 311 V, which is rectified voltage rating of 220 V_{rms} at 60 Hz. A flyback converter with an integrated pulse width modulation (PWM) controller is used to step down 311 V to 5 V and 12 V, which supplies auxiliary power to the MCU, communication circuit and driver. A MCU (AT90PWM) is mainly used to control the operation of the power transfer between the coils. It changes the transfer frequency according to the received data from the communication circuits. A half-bridge inverter is used to drive the primary coil, where the source is the 311-V bus after the full bridge rectifier. Between the rectifier and inverter, a MOSFET (M_1) is placed to prevent shoot-through current while changing the driver frequency of the primary coil. The MOSFET is needed because gate signals for M_2 and M_3 become high when the MCU changes the frequency.

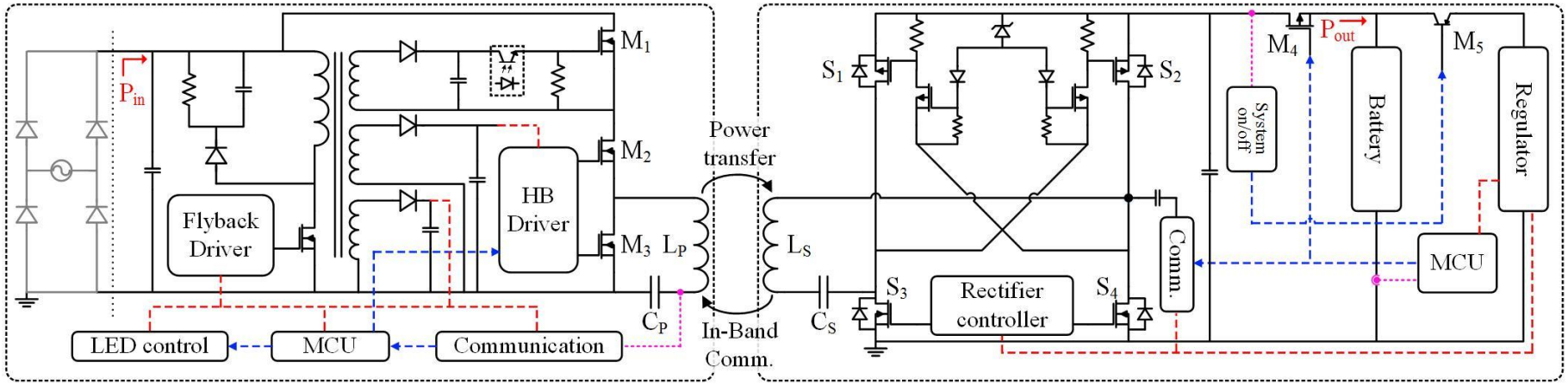

Fig. 3-11. Proposed wireless battery charger schematic (red dots line: low level power line, blue dots line: control line, purple dots line: sensing line).

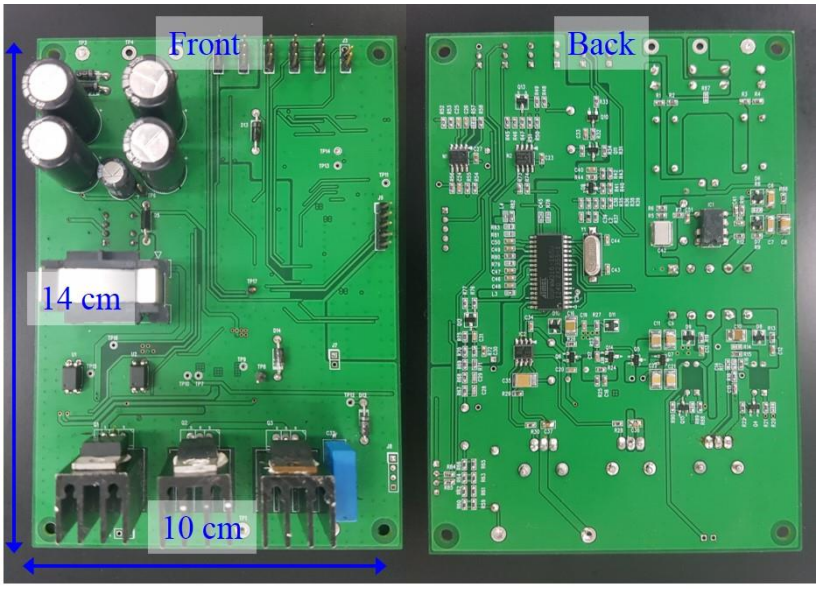

(a)

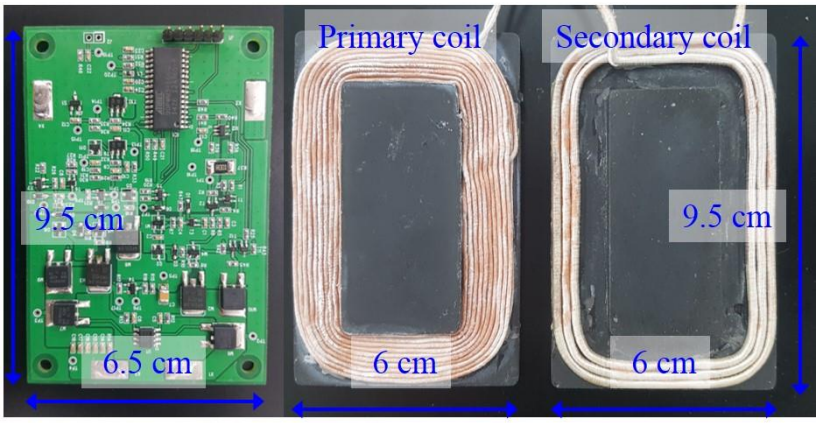

(b)

Fig. 3-12. Fabricated adaptive frequency modulation technique IPT system. (a) Primary side circuit. (b) Secondary side circuit, primary and secondary coils.

The secondary side schematic is also shown in in Fig. 3-11. The secondary side PCB is shown in Fig. 3-12 (b). The secondary side is made up of a full-bridge active rectifier, regulators, and an MCU. The active rectifier converts transferred ac power into dc power. This active rectification circuit decreases drop-out voltage compared to a diode rectifier from about 700 mV to 100 mV, which increases conversion efficiency. The system on/off circuit is triggered when the primary side sends power. After checking the signal, the system on/off circuit turns on MOSFET M_4 and BJT M_5 to charge the battery and turn on the MCU. This circuit makes reduce standby power by selectively turning on the MCU.

The MCU plays a main role in the receiver as it processes all the monitored data. It senses the battery identification resistor to determine whether or not the connected battery is compatible with the charging system.

It monitors the voltage and current to control the charging state. In addition, the monitored data are used for over-voltage protection and over-current protection.

3.4.2. Coils characteristics

The primary coil is 9.5 × 6 cm^2 in size and consists 33 turns with a total inductance of 264 μH. The secondary coil is 9.5 × 6 cm^2 size and consists of 3 turns with a total inductance of 3.1 μH. The gap between primary and secondary coils is 7 mm during power transfer. Fig. 3-13 shows measured efficiency from the primary to secondary coils. This was measured with a network analyzer (Keysight E5061B ENA), which supports power transfer efficiency measurements for wireless power transfer applications. The power transfer efficiency is above 95% in the 130-160 kHz range. This result is well-matched with 95.0% - 95.2%, which is the calculated efficiency using efficiency equations in [3-6]. Because of the low-quality factor, the power efficiency is almost constant over a broad frequency range. This characteristic is suitable for the proposed frequency modulation technique.

Parameters		Value
Primary side	Primary board size	14 × 10 cm^2
	Primary coil size	9.5 × 6 cm^2
	L_p	264 μH
	C_p	8.2 nF
	V_{in}	311 V_{ac}
	Major components	MCU (AT90PWM), Driver IC (IRS2186), Half bridge inverter (IPP60R230P6)
Secondary side	Secondary board size	9.5 × 6.5 cm^2
	Secondary coil size	9.5 × 6 cm^2
	L_s	3.1 μH
	C_s	700 nF
	V_{out}	16 - 20.75 V
	Major components	MCU (AT90PWM), Rectifier (IRFR8314PbF, IPD90P03PAL), Rectifier controller (TEA1795T)

Table 3-1. System parameter and major components

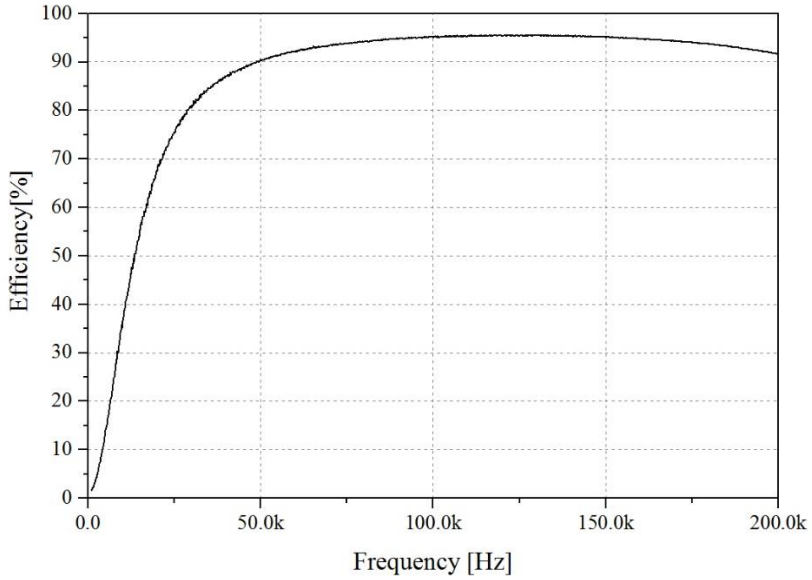

Fig. 3-13. Measured primary to secondary coil efficiency.

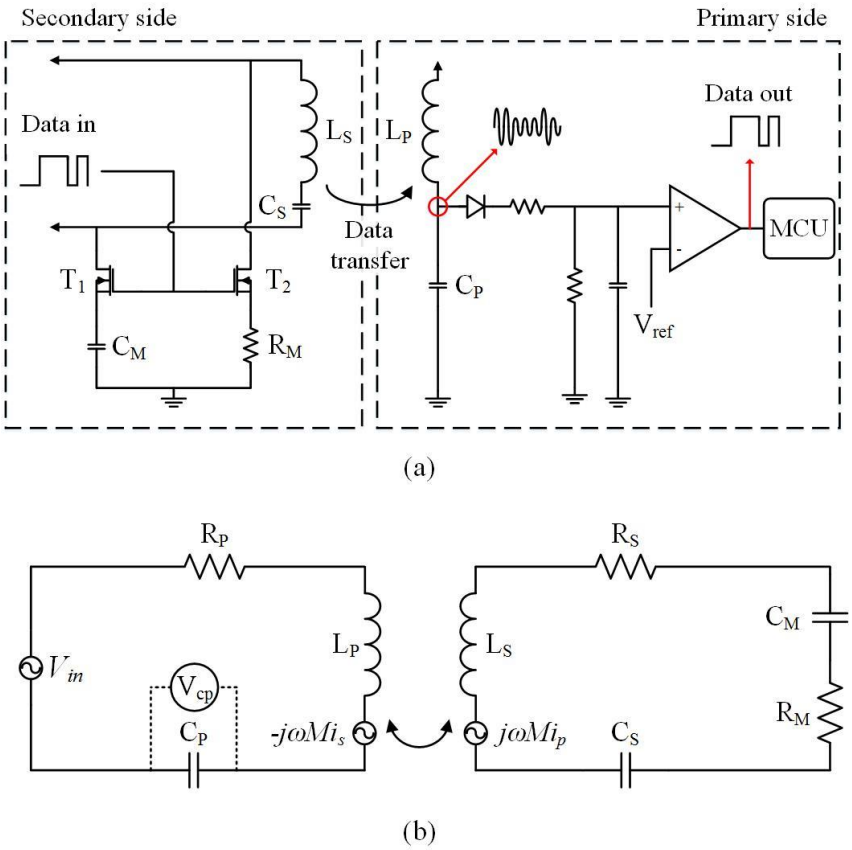

Fig. 3-14. In-band communication circuits. (a) Block diagram. (b) Equivalent circuit.

3.4.3. Communication circuit and analysis

The basic concept of in-band communication is introduced in [3-7] used for IPT, but is not widely covered in the literature. In this section, the in-band communication is analyzed using equivalent circuit. Fig. 3-14(a) shows the communication circuit of the primary and secondary side, where unidirectional in-band communication is used. The data are transferred from the secondary to primary side. An impedance modulation technique is used for the in-band communication. MOSFETs (T_1, T_2) are connected to L_S and C_S to make a path to C_M and R_M, which changes the impedance of the secondary side. When T_1 and T_2 are turned on, the primary side also senses the impedance change of the secondary side. The voltage between L_P and C_P is changed. During communication, the equivalent circuit is represented as Fig. 3-14(b). The impedance of the primary side is the same as (1), but the secondary side is expressed as

$$Z_s = j\omega L_s + \frac{1}{j\omega C_s || C_M} + R_s + R_M \tag{3.6}$$

where C_M is the capacitor for impedance modulation and R_M is the resistance for impedance modulation.

$$i_p = \frac{V_{in}}{Z_p + \omega^2 M^2 / Z_s} \tag{3.7}$$

Equation (7) is the current (i_p) of the primary side. The voltage of C_P can be expressed as

$$V_{cp} = \frac{1}{\omega C_p} i_p \tag{3.8}$$

Based on (3.7) and (3.8), the voltage results of the C_P over frequency are shown in Fig. 3-15. The top black line shows V_{cp} without data transferring. The bottom red line shows V_{cp} with data transferring. These high voltage signal are rectified and stepped down to below 5 V. Then, a voltage comparator is used to restore the data and send it to the MCU. The voltage difference makes data recognizable. With this communication technique, the secondary side can send data immediately when an event occurs. Fig. 3-16 shows the measured results during communication. The blue line (top trace) shows the sending data signal from the secondary side. Since in-band communication is performed while the primary side still tries to transfer power, some noise is observed in the sending signal. The light blue line (middle trace), shown in the middle of Fig. 3-16, is the voltage of C_P. In the figure, the parts indicated by the arrows are the voltage change due to the data. The yellow colored line (bottom trace) is the recovered data at the primary side. Even with some noise on the sending side, the restored date on the primary side is accurately received.

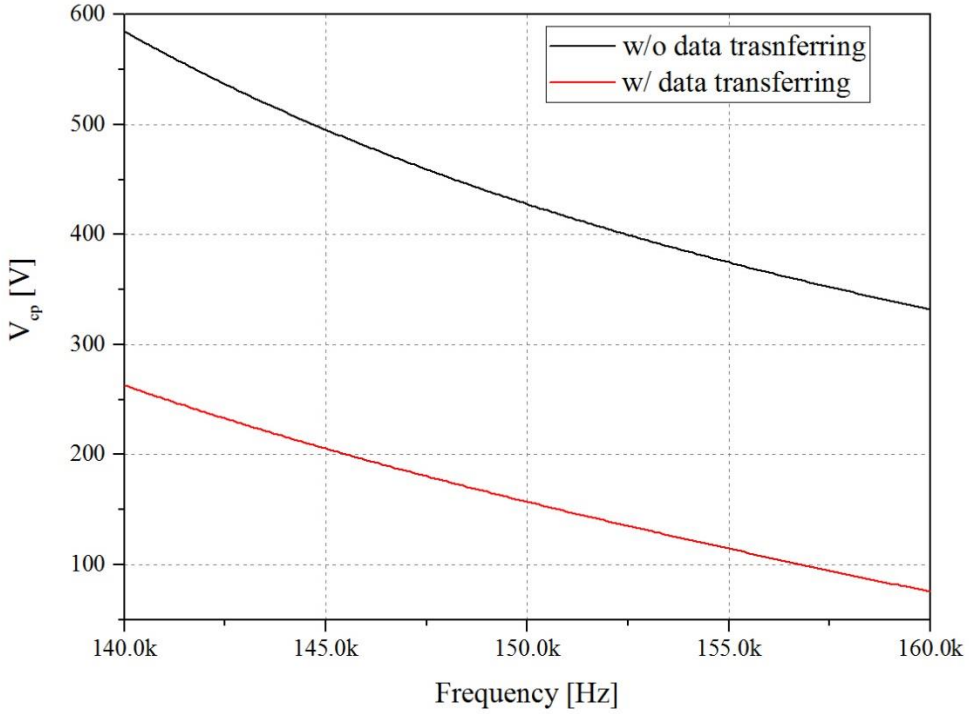

Fig. 3-15. Voltage of the C_P when communicated depending on frequency.

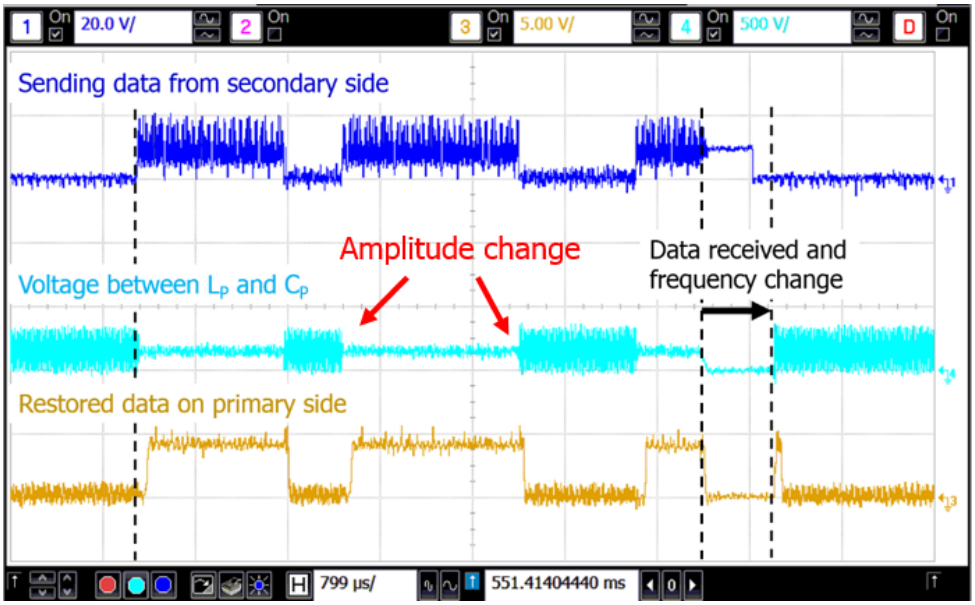

Fig. 3-16. Measured communication signal at primary and secondary side.

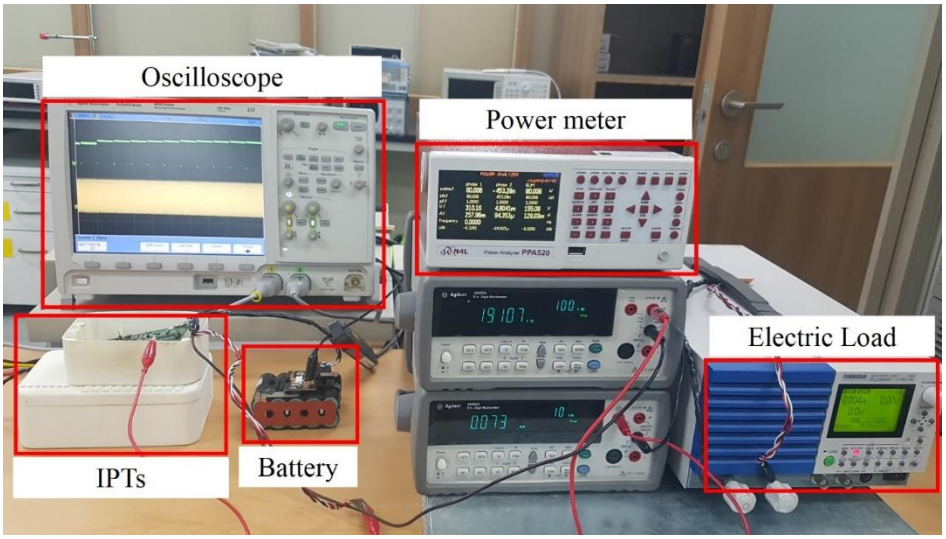

Fig. 3-17. Experimental setup.

3.5. Experimental verification

3.5.1. Experimental setting

The proposed adaptive frequency modulation technique provides a way to track the optimal coil transfer frequency to charge the battery based on its voltage conditions. Fig. 3-17 shows the experimental setup of the proposed wireless battery charger. The proposed system is measured using a power supply (Kikusui PCR2000LA), electric load (Kikusui PLZ334W), oscilloscope (Lecory HDO4000A, Kesight MSO9254A), and power analyzer (N4L PPA520).

3.5.2. Measured results

The input voltage of the system is 311 V, which is the rectified voltage rating of the 220 V_{rms} A. The used battery profile is shown in Table 3-2. The nominal voltage of each cell is 3.6 V and the charge current is 2A for long cycle use. Maximum charging voltage is 4.15 V for long cycle charge. 5S2P Li-ion battery (5 cells in series, 2 cell strings in parallel) is used for charging test. Fig. 3-18 shows the used 5S2P Li-ion battery.

Item	**Specification**
Nominal voltage	3.6V
Standard charge	CCCV, 1A, 4.20 ± 0.05 V
Rapid charge	CCCV, 4A, 4.20 ± 0.05 V
Long cycle charge	CCCV, 2A, 4.10 ± 0.05 V

Table 3-2. 1 cell Li-ion battery profile

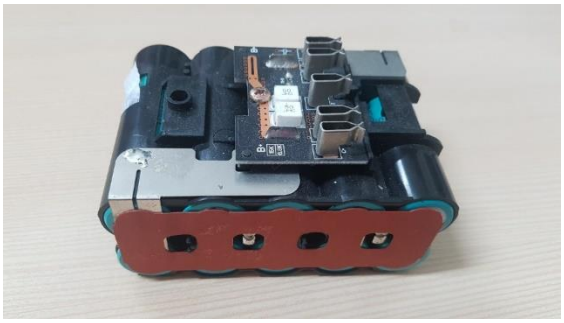

Fig. 3-18. 5S2P Li-ion battery.

In Fig. 3-19, the measurement waveform of the proposed IPT system is shown when the transfer frequency is 148 kHz and charging power is 78.5 W. The upper waveform is the voltage and current at the primary side, and the lower waveform is the voltage and current at the secondary side before rectification. The secondary side maximum voltage is equivalent to the battery voltage and the system charges the battery in CC mode.

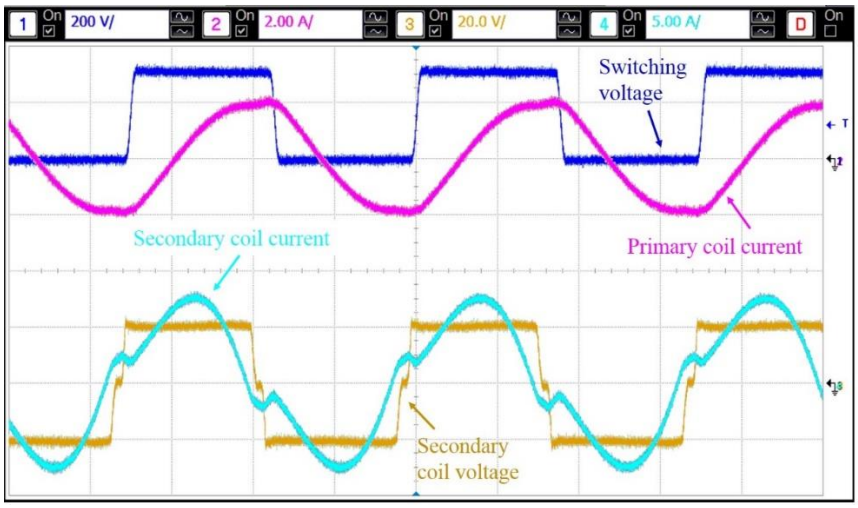

Fig. 3-19. Measured waveforms of the proposed IPT. (148-kHz and 78.5-W output power).

Fig. 3-20 shows the measured power transfer efficiency, charging current, and charging frequency over the output power range. The efficiency is measured from the dc input power P_{in} to the battery charging power P_{out}, which is indicated in Fig. 3-11, such that efficiency is $\eta = P_{out}/P_{in}$. Fig. 3-20(a) shows the charging efficiency of the system under CC mode at 4-A charging current. The average efficiency is 89.5% under 66-87 W charging conditions. In CC mode, the voltage of the battery increases with the charging power. The maximum efficiency is 90.3% under a 68-W charging condition Fig. 3-20 (b) shows the charging efficiency of the system under CV mode with the battery voltage at 20.75 V. The maximum and minimum efficiencies in CV mode are 89.7% and 68.3%, respectively.

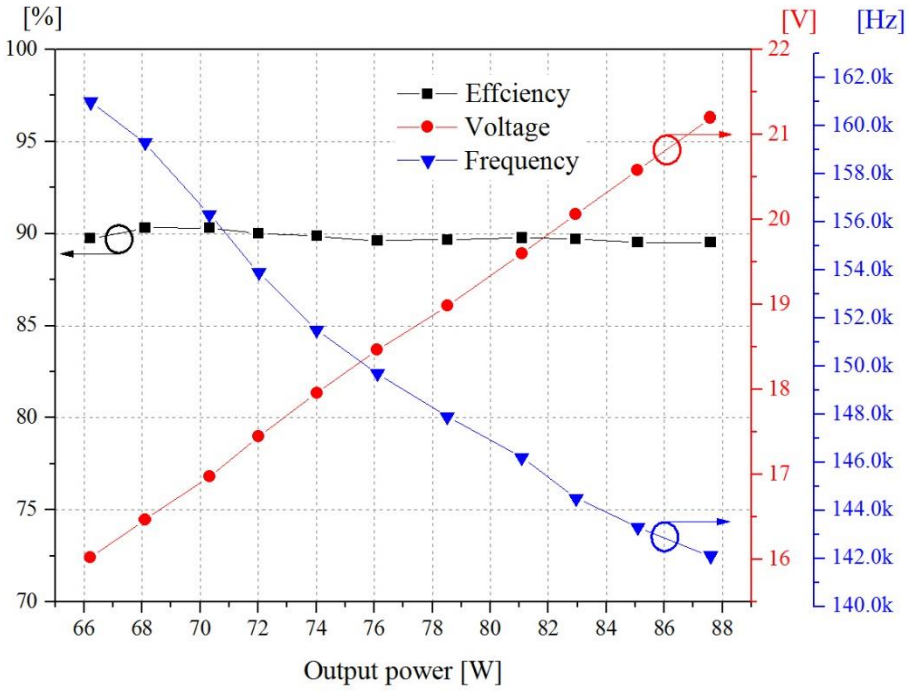

(a)

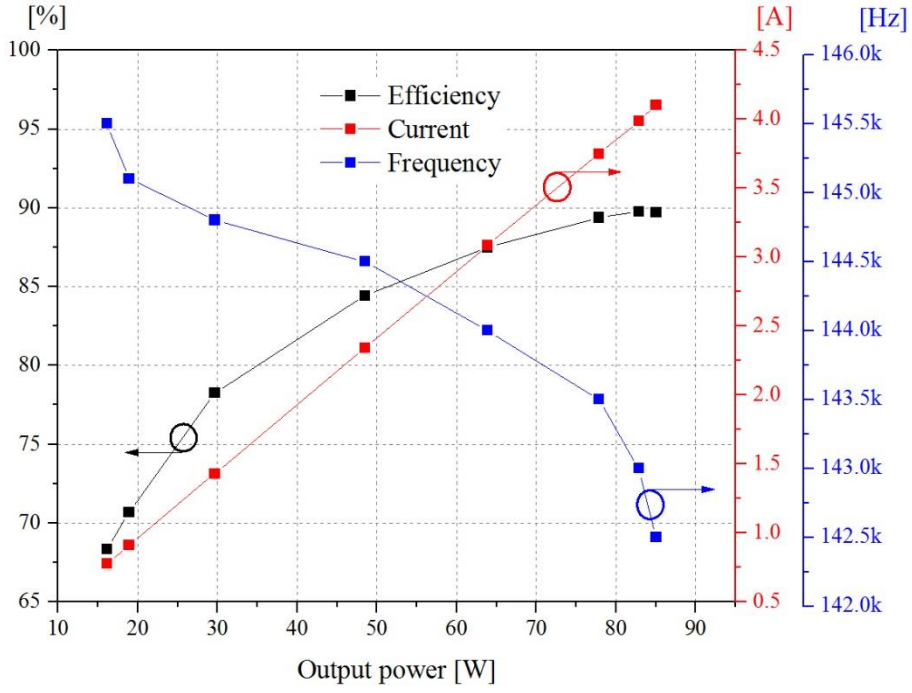

(b)

Fig. 3-20. Charing efficiency profile with transfer frequency and battery voltage or charging current. (a) CC mode profile. (b) CV mode profile.

Fig. 3-21 shows the battery charging waveforms of the proposed wireless battery charger in the time domain. The top pink line indicates charging voltage, and the bottom yellow line indicates charging current. This is measured with oscilloscope, which support long time roll mode measuring. Total charging time is 62 minutes. The average charging current is 4 A in CC mode. The transfer frequency is determined by the proposed algorithm and controlled discreetly with the MCU. The transfer frequency range is 142-162 kHz. Battery is charged from the minimum voltage of the maximum voltage. In the experiment, a Li-ion battery is used, and the battery is charged from the minimum voltage to the maximum voltage. Fig. 3-21 shows the charging characteristics of the CC/CV mode by using “step charging method” without a regulator. This result shows that “step charging method” can be used in other frequency controllable IPT systems with in-band communication.

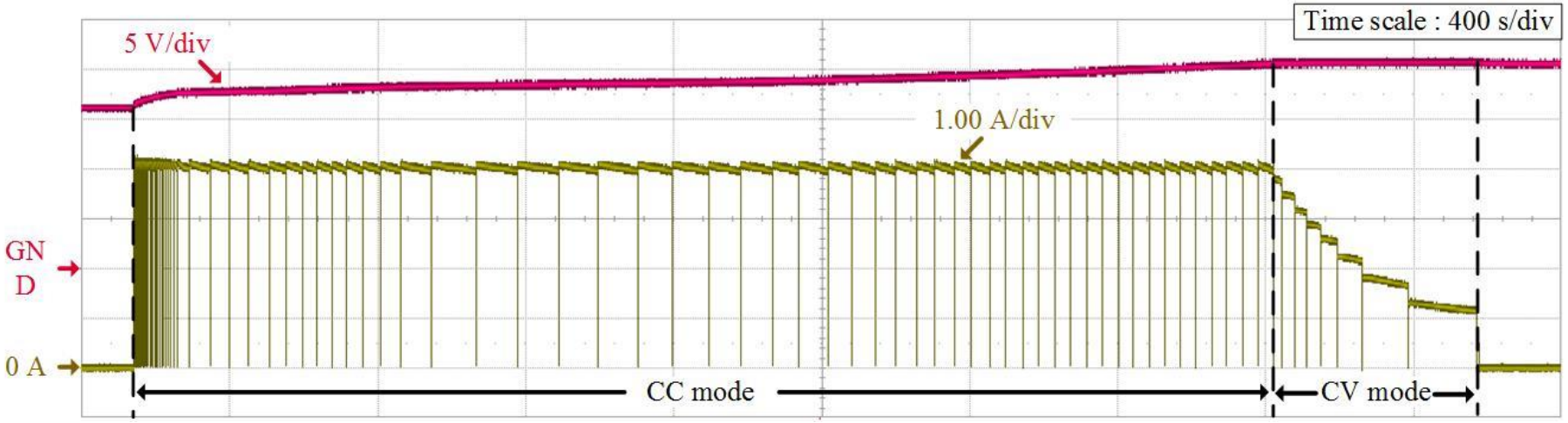

Fig. 3-21. Measured CC/CV mode battery charging profile in time domain.

	Distance	Eff.	Power	System feature			
				Feedback comm.	CC/CV mode control	Remark	Power stage
[3-8]	On pad	63%	2.5 W	In-band comm.	Freq. modulation, Regulator	Continuous feedback (conventional)	4
[3-9]	On pad	84%	15 W	In-band comm.	Freq. modulation, Regulator	Continuous feedback (conventional)	4
This work	0.7 cm	90.3%	80 W	In-band comm.	Freq. modulation	**Step charging method**	***3***

Table 3-3. Comparison table of IPT systems with in-band communication

Table 3-3 shows the performance comparison of IPT systems using in-band communication. Other IPT techniques using in-band communication regulate power using an LDO regulator as well as frequency modulation [3-8, 3-9]. To minimize the dropout voltage in the regulator, the frequency is frequently adjusted. The cycle is about 250 ms. The maximum loss power is about 250 mW, which is about 5% loss in 5W power system. This method can be applied to IPT system using in-band communication. When proposed “step charging method” is applied to the IPT, the loss of the regulator is eliminated, and the efficiency is increased. The result is a method that increases the efficiency by reducing the loss of Rx (implanted devices), so it will have less temperature of device of and is suitable for biomedical.

3.6. Summary

This chapter presented a new step charging method to regulate battery charging voltage and current with minimized power stages in frequency controllable IPT system using in-band communication. The frequency modulation technique and in-band communication mechanism have been analyzed and demonstrated. To charging with step charging method, voltage hysteresis of the rechargeable battery was used. Then, experiment verification was performed to confirm the step charging method. To demonstrate step charging method, the hardware implementation is designed for an 90.3 % efficiency IPT charging system using in-band communication. The power stages consist of half-bridge inverter, coil link and active rectifier. As shown in the algorithm, CC / CV mode charging was also possible in the IPT system without extra battery charger such as DC-DC converter or LDO regulator. The number of times the communication was performed for 62 minutes is 200 times, so that it can be controlled with a very small number of feedbacks compared to the existing method communicates at every 250 ms. This result shows that it is possible to regulate the voltage without the extra battery charger and it shows that this algorithm is applicable to the IPT system. This efficiency improvement shows that it can be used more safely in human body.

Chapter IV

Summary & Conclusion

In this thesis, the proposed power control techniques in MR-WPT and IPT systems are presented and demonstrated. WPT efficiency in biomedical applications is a critical issue because of the safety in usage. In the low-efficiency WPT system, it is necessary to increase the radiated power, so that the SAR is increased, which indicates that the human body temperature is raised by the radiated electromagnetic waves. Due to low efficiency, the device temperature rises. Since increasing the temperature of human tissues is a factor that can cause cancer, it is the most avoidable factor for wireless power transmission in biomedical applications.

The efficiency degradation problem caused by change of geometric position and small coil size, which is limited by application is presented and analyzed for biomedical application such as capsule endoscopy. However, WPT system is required for convenient patients. To solve the efficiency degradation, coupling coefficient control technique for optimal efficiency is presented with variations in the distance, angle, and axial-misalignment to the transmitter. This power control technique utilizes the coupling coefficient k_{12}. Controlling k_{12} is a good parameter to use for biomedical applications because it is controlled in an external Tx system. It was demonstrated experimentally that the proposed MR-WPT system can track the optimal efficiency under various geometric factors.

The variable load problem is presented in wireless power transfer system for battery charging. In order to charge the battery in CC/CV mode, the power stage is increased more than the existing wire method, and this comes down to efficiency reduction. Among them, IPT system uses frequency modulation and regulator to implement CC/CV mode, which is caused by efficiency decrease and temperature increase in Rx devices. To increase the power transfer efficiency, the step charging method in frequency controllable IPT system using in-band communication is presented and demonstrated. Use the voltage hysteresis of battery to charge, battery is charged stepwise. This method can be used to charge with a charging current in CC mode with little error. The charging voltage does not exceed the maximum value by using stepwise reduced current. In this way, battery is charged up to the maximum capacity. Proposed “step charging method” allows design without a regulator, loss caused by regulator is eliminated.

In this thesis, two power control techniques are proposed and demonstrated for increased efficiency in biomedical applications. These power control techniques are promising technologies that can help WPT to be integrated and commercialized in biomedical devices.

References

[1-1] W.C. Brown, “The History of Wireless Power Transmission”, Solar Energy, Jan. Vol. 56, No.1, pp. 3-21, 1996.

[1-2] N. Tesla, “Apparatus for transmission of electrical energy”, US Patent, May, No.649621, 1900.

[1-3] A. KURS, A. KARALIS, R. MOFFATT, J. D. JOANNOPOULOS, P. FISHER, M. SOLJAČIĆ, “Wireless Power Transfer via Strongly Coupled Magnetic Resonances”, SCIENCE 06 JUL 2007 : 83-86

[1-4] https://www.wirelesspowerconsortium.com/

[1-5] R. N. Fogoros, MD, a board-certified physician, “What You Should Know About Pacemakers”, October 23, 2017.

[1-6] ICNIRP, “Guidelines for limiting exposure to time-varying electric, magnetic, and electromagnetic fields (up to 300 GHz),” Health Phys., vol. 74, pp. 494–522, 1998.

[1-7] T. Ishiyama, et al., “Impact of a wireless power transmission system using an ultrasonic air transducer for low-power mobile applications”, Ultrasonics, 2003 IEEE Symposium on , vol.2, no., pp. 1368- 1371.

[1-8] H. Hu, Y. Hu, C. Chen, and J. Wang, “A system of two piezoelectric transducers and a storage circuit for wireless energy transmission through a thin metal wall”, IEEE Transactions on Ultrasonics, Ferroelectrics and Frequency Control, vol.55, no.10, pp.2312-2319, 2008.

[1-9] T. Blackwell, “Recent demonstrations of laser power beaming at DFRC and MSFC”, Third International Symposium on Beamed Energy Propulsion, AIP Conference Proceedings, vol.766, pp.73-85, 2005.

[1-10] H. Matsumoto, “Research on solar power satellites and microwave power transmission in Japan”, Microwave Magazine, IEEE, vol.3, no.4, pp. 36- 45, 2002.

[1-11] J. Benford, “Space applications of high-power microwaves”, IEEE Transactions on Plasma Science, June, Vol.36, No.3, pp.569-581, 2008.

[1-12] IEEE-SA Standards Board, “IEEE standard for safety levels with respect to human exposure to radio frequency electromagnetic fields, 3kHz to 300GHz”, IEEE Std. C95.1, 2010

[1-13] S. C. Thierauf, “High-speed Circuit Board Signal Integrity”, p.56, Artech House, 2004 ISBN 1580538460.

[1-14] S. Kim, S.A. Kim, G. Jung, K. Kwon and J. Chun, “Design of a reliable broadband I/O employing T-coil”, Journal of Semiconductor Technology and Science, vol. 9, no. 4, pp. 198-204, 2009.

[1-15] K. A. Grajski, R. Tseng and C. Wheatley, “Loosely-coupled wireless power transfer: Physics, circuits, standards”, IEEE MTT-S International Microwave Workshop Series on Innovative Wireless Power Transmission: Technologies, Systems, and Applications, Kyoto, 2012, pp. 9-14.

[1-16] Y.-H. Kim, S.-Y. Kang, M.-L. Lee, B.-G. Yu, and T. Zyung, “Optimization of wireless power transmission through resonant coupling,” Compat. Power Electron., pp. 426–431, May 2009.

[1-17] A. H. Mohammadian, E. T. Ozaki, and M. S. Grob, “Repeaters for Enhancement ofWireless Power Transfer,” U.S. Patent 2009/0286470, Nov. 19, 2009.

[1-18] T. P. Duong, and J. W Lee, “Experimental Results of High-Efficiency Resonant Coupling Wireless Power Transfer Using a Variable Coupling Method,” IEEE Microwave and Wireless Components Letters, vol.21, no.8, pp.442-444, Aug. 2011.

[1-19] H. Hoang, S. Lee, Y. Kim, Y. Choi, and F. Bien, "An Adaptive Technique to Improve Wireless Power Transfer for Consumer Electronics," IEEE Trans. Cons. Electron., vol. 58, no. 2 pp. 327-332, May 2012.

[1-20] A. Zaheer, G. A. Covic and D. Kacprzak, "A Bipolar Pad in a 10-kHz 300-W Distributed IPT System for AGV Applications," in IEEE Transactions on Industrial Electronics, vol. 61, no. 7, pp. 3288-3301, July 2014

[1-21] R. Bosshard, J. W. Kolar and B. Wunsch, "Control method for Inductive Power Transfer with high partial-load efficiency and resonance tracking," 2014 International Power Electronics Conference, Hiroshima, 2014, pp. 2167-2174.

[1-22] C. C. Hua, H. R. Chen and Y. H. Fang, "Inductive power transmission technology for Li-ion battery charger," *2013 IEEE 10th International Conference on Power Electronics and Drive Systems (PEDS)*, Kitakyushu, 2013, pp. 788-792.

[1-23] R. Mai, Y. Chen, Y. Li, Y. Zhang, G. Cao, and Z. He, “Inductive power transfer for massive electric bicycles charging based on hybrid topology switching with a single inverter,” IEEE Trans. Power Electron., vol. 32, no. 8, pp. 5897–5906, Aug. 2017.

[1-24] M. Galizzi, M. Caldara, V. Re and A. Vitali, "A novel Qi-standard compliant full-bridge wireless power charger for low power devices," 2013 IEEE Wireless Power Transfer (WPT), Perugia, 2013, pp. 44-47.

[1-25] B. Johns, “An introduction to the Wireless Power Consortium standard and TI’s compliant solutions”, Analog Applications Journal, 1Q 2011, pp. 10-12.

[2-1] P. Swain, "Wireless capsule endoscopy," Gut, vol. 52, no. 4, pp. 48-50, Jun. 2003.

[2-2] G. Iddan, G. Meron, A. Glukhovsky, and P. Swain, "Wireless capsule endoscopy," Nature, vol. 405, no. 6785, pp. 417, May. 2000.

[2-3] A. Moglia, A. Menciassi, M. O. Schurr, and P. Dario, "Wireless capsule endoscopy: from diagnostic devices to multipurpose robotic systems," Biomed. Microdevices, vol. 9, no. 2, pp. 235-243, Apr. 2007.

[2-4] P. Swain, "The future of wireless capsule endoscopy," World J. Gastroenterology, vol. 14, no. 26, pp. 4142-4145, Jul. 2008.

[2-5] A. Moglia, A. Menciassi, P. Dario, and A. Cuschieri, "Capsule endoscopy: progress update and challenges ahead," Nat. Rev. Gastroenterology & Hepatology, vol. 6, pp. 353-362, Jun. 2009.

[2-6] R. Chávez-Santiago, I. Balasingham, and J. Bergsland, "Ultrawideband Technology in Medicine: A Survey," J. Electrical and Computer Engineering, vol. 2012, pp. 9, 2012.

[2-7] K. C. Kong, J. Cha, D. Jeon, and D. I. D. Cho, "A rotational micro biopsy device for the capsule endoscope," in IEEE/RSJ Int. Conf. IROS, 2005. pp.1839-1843.

[2-8] S. Park, K. I. Koo, S. M. Bang, J. Y. Park, S. Y. Song, and D. Cho, "A novel microactuator for microbiopsy in capsular endoscopes," J. Micromech. Microeng., vol. 18, no. 2, pp. 9, Feb. 2008.

[2-9] M. Quirini, S. Scapellato, P. Valdastri, A. Menciassi, and P. Dario, "An approach to capsular endoscopy with active motion," in IEEE Ann. Int. Conf. EMBS, Lyon, 2007, pp. 2827-2830.

[2-10] R. Puers, R. Carta, and J. Thone, "Wireless power and data transmission strategies for next-generation capsule endoscopes," J. Micromechanics and Microengineering, vol. 21, p. 15, May. 2011.

[2-11] K. A. Grajski, R. Tseng, and C. Wheatley, "Loosely-coupled wireless power transfer: Physics, circuits, standards," in IEEE MTT-S IMWS, Kyoto, Japan., 2012, pp. 9–14.

[2-12] K. Kadota, "Designing wireless power supply systems," ANSYS, Inc., ANSYS Advantage, vol. 5, no 3, pp.38-40 2011.

[2-13] S. Kim, J. S. Ho, L. Y. Chen, and A. S. Y. Poon, “Wireless power transfer to a cardiac implant,” Appl. Phys. Lett., vol. 101, pp. 073701-1–073701-4, Aug. 2012.

[2-14] A. S. Y. Poon, “Electromagnetic field focusing for short-range wireless power transmission,” in 6th IEEE Radio Wireless Week Symp., Santa Clara, CA, U.S., Jan. 15–18, 2012, pp. 115–118.

[2-15] D. Balaguru, U. Bhalala, M. Haghighi, and K. Norton, "Computed tomography scan measurement of abdominal wall thickness for application of near-infrared spectroscopy probes to monitor regional oxygen saturation index of gastrointestinal and renal circulations in children," Pediatr. Crit. Care Med., vol. 12, pp. E145-E148, May. 2011.

[2-16] V. De Santis, P. A. Beeckman, D. A. Lampasi, and M. Feliziani, "Assessment of Human Body Impedance for Safety Requirements Against Contact Currents for Frequencies up to 110 MHz," IEEE Trans. Biomed. Eng., vol. 58, no. 2, pp. 390-396, 2011.

[2-17] ICNIRP, “Guidelines for limiting exposure to time-varying electric and magnetic fields (1 Hz to 100 kHz),” Health Phys., vol. 99, pp. 818–836, 2010.

[2-18] IEEE Standard for Safety Levels With Respect to Human Exposure to Electromagnetic Fields, 0–3 kHz, IEEE Standard C95.6, 2002.

[2-19] IEEE Standard for Safety Levels With Respect to Human Exposure to Radiofrequency Electromagnetic Fields, 3 kHz to 300 GHz, IEEE Standard C95.1, 2005

[3-1] R. Steigerwald, "A comparison of half-bridge resonant converter topologies," IEEE Trans. Power Electron., vol. 3, no. 2, pp. 174–182, Apr. 1988.

[3-2] R. Chen, C. Zheng, Z. U. Zahid, E. Faraci, W. Yu, J.-S. Lai, M. Senesky, D. Anderson, and G. Lisi, "Analysis and parameters optimization of a contactless IPT system for EV charger," in Proc. IEEE Appl. Power Electron. Conf. Expo., Mar. 16-20, 2014, pp. 1654–1661.

[3-3] R. Bosshard, J. W. Kolar, and B. Wunsch, "Control method for inductive power transfer with high partial-load efficiency and resonance tracking," in Proc. Int. Power Electron. Conf., Hiroshima, Japan, May 18-21, 2014, pp. 2167–2174.

[3-4] Half bridge resonant LLC converters and primary side MOSFET selection, AN4720. [Online]. Available: http://www.st.com/resource/en/application note/dm00207043.pdf

[3-5] W. Dreyer and P. Friz, "Stochastic methods for the analysis of lithium-ion batteries", [Online]. Available: http://www.wias-berlin.de/projects/ECMath-SE8/

[3-6] P. Si, A. P. Hu, S. Malpas, and D. Budgett, "A frequency control method for regulating wireless power to implantable devices," IEEE Trans. Biomed. Circuits. Syst., vol. 2, no. 1, pp. 22–29, Mar. 2008.

[3-7] WPC v1.2 wireless power transmitter manager with 15-W power delivery, bq501210. [Online]. Available: http://www.ti.com/lit/ds/symlink/bq501210.pdf

[3-8] J. T. Hwang, D. S. Lee, J. H. Lee, S. M. Park, K. W. Jin, M. J. Ko, H. I. Shin, S. O. Jeon, D. H. Kim, and J. Rhee, "21.8 an all-in-one (Qi, PMA and A4WP) 2.5W fully integrated wireless battery charger IC for wearable applications," in IEEE Int. Solid-State Circuits Conf. (ISSCC), Jan. 31-, Feb. 4, 2016, pp. 378–380.

[3-9] WPC Qi v1.2-compliant, Wireless Power Receiver and Battery Charger bq5105xB. [Online]. Available: http://www.ti.com/lit/ds/symlink/bq51051b.pdf

Acknowledgement

학위 과정 동안 저를 항상 격려해 주시고 지도해주신 변영재 교수님께 깊은 감사를 드립니다. 미숙하였던 제가 교수님의 학문적, 기술적 지도를 받아 연구 결과를 낼 수 있었습니다. 앞으로의 제 인생에서 많은 도움과 지침이 될 것이라 의심치 않습니다. 아울러 바쁘신 중에 저의 논문 심사를 해주시기 위해 소중한 시간을 할애해 주신 김진국 교수님, 김예린 교수님, 김성진 교수님 한기진 교수님께도 감사의 인사 드립니다.

박사 과정 중 함께 해왔던 BICDL 연구실 멤버 모두에게 감사의 인사를 전합니다. 처음 연구실에 왔을 때 많은 것을 알려준 윤호형, 연구를 함께 하였고 최고의 친구인 Sai Kiran Oruganti, 가장 오랜 시간 함께한 상현이, 부천고 선배이며 UNIST에서 새로운 인연으로 만난 희돈이형, WPT 연구팀에 합류해 힘든 시간을 함께 보낸 형근이 덕분에 힘든 시간을 버틸 수 있었습니다. 먼저 졸업한 패션리더 기롬이, 그리고 앞으로 큰형 될 복서 주협이, 항상 부지런한 박경민이, 앞으로 우리 연구실 차세대 동력 에이스 우진이, 낙천적인 은호, 오타쿠 경호, 귀염둥이 본영이, 화석 석태, 엉뚱한 낙영이, 철인 성문이, 미식가(?) 성규, 새로 연구실에 합류한 현경이, 새로운 Indian 멤버 Malik 덕분에 연구실에서 즐겁게 보낼 수 있었습니다.

연구실 초기에 힘든 시기를 같이 술로 버텨준 동욱이, 초기 후기 항상 함께해준 명환이, 연구실의 라이벌 경환이, GIST 시절부터 오랜 시간 함께한 요한이, 저에게 연구 도움도 많이 준 연구를 숨쉬는 것처럼 하는 진정한 연구자 동일이에게 고맙다는 말을 전하고 싶습니다.

우연인지 운명인지 같이 울산에 오게 된 규진이 덕분에 타지 생활이 한결 마음이 편했습니다. 엉뚱한 장난으로 즐거움을 줬던 승환이, 우리 한양대 전통컴 동기 용신이, 상민이, 대건이, 병준이, 강윤이, 원영이, 먼 거리에 있었지만 항상 곁에 있는 거 같은 친구들 덕분에 든든했습니다.

긴 대학원 생활 동안 항상 힘이 되어주었던 아버지, 어머니, 선정이 우리 가족 모두 사랑하고, 고맙습니다.

이제 대학원 생활을 마무리하고, 지난 6년을 머물렀던 울산을 떠나게 됩니다. 뒤를 돌아보니 아쉬움이 많이 남지만, 사회에 첫 발 내딛고 더 큰 도약을 준비합니다. 다시 한번 저를 이끌어 주신 모든 분들께 감사 드립니다.

Curriculum Vitae

Personal

Name: Kyung min Na (나 경 민, 羅 敬 玟)

Education

2012.3 – 2018.2 Ph. D. in Department of Electrical Engineering

Ulsan National Institute of Science and Technology (UNIST), Ulsan, Korea.

Major: Wireless Power Transfer System

Thesis Title: *Power Control Techniques in Wireless Power Transfer System*

Advisor: Prof. Franklin Bien

2010.3 – 2012.2 M.S. in Department of Nanobio Material and Electronics

Gwangju Institute of Science and Technology (GIST), Gwangju, Korea.

Major: Magnetic thin films

Thesis Title: *Magnetization reversal of CoFe/Tb multilayer by femtosecond laser*

Advisor: Prof. Beongki Cho

2006.3 – 2010.2 B.S. in Department of Electrical & Computer Engineering

Hanyang University. Seoul, Korea

Major: Electrical & Computer Engineering

Project Experiences

- “자가충전형 초소형 전국단위 위치추적 시스템 원천기술개발”, 2017.09 – 2017.12, 대학ICT연구센터 (ITRC)
- “스텐트 기반 체내이식형 혈당측정 마이크로 시스템 연구”, 2016.03 – 2017.12, 울산과학기술원 연구성과사업화과제
- “안테나 락-루프(ALL) 기반 실시간 어뎁티브 3차원 코드리스 파워존”, 2014.05 – 2017.04, 미래창조과학부 핵심연구과제
- “자기 유도형 무접점 전력전송 및 베터리 충전 시스템 개발”, 2015.07 – 2016.07, (주)계양전기
- “Flexible TSP controller IC 기술개발”, 2012.05 – 2014.01, (주)삼성디스플레이

Publications

[1] **K. Na**, H. Ma, J. Park, J. Yeo, F. Bien, "Graphene-Based Wireless Environmental Gas Sensor on PET Substrate," IEEE Sensors Journal, Volume:16, Issue: 12, Page(s): 5003 - 5009, 18 February 2016

[2] **K. Na**, H. Jang, H. Ma, Y. Choi and F. Bien, "A 200 Mbps Data Rate 3.1-4.8 GHz IR-UWB All-Digital Pulse Generator with DB-BPSK Modulation," IEEE Transaction on Circuit and System (T-CAS) II, Volume:62, Issue 12, Page(s): 1184 - 1188, Aug. 14, 2015

[3] **K. Na**, Franklin Bien, "Tracking Optimal Efficiency of Magnetic Resonance Wireless Power Transfer System for Biomedical Capsule Endoscopy", IEEE Transactions on Microwave Theory and Techniques, Vol. 63, No. 1, pp.295-304, Jan. 2015

[4] H. Ma, Z. Liu, S. Heo, J. Lee, **K. Na**, H.B. Jin, S. Jung, K. Park, J.J. Kim, and F. Bien, "On-Display Transparent Half-Diamond Pattern Capacitive Fingerprint Sensor Compatible with AMOLED Display", IEEE Sensors Journal, Volume: 16, Issue: 22, Page: 8124 – 8131, 1 September 2016

[5] K. Lee, J. Park, M.S. Lee, D. Kang, **K. Na**, C. Lee, F. Bien, J. Park, "In-situ Synthesis of Single Walled Carbon Nanotube-Graphite Electronic Devices and Their Integrations with Nature's Life Forms," the Nano Letters, ACS Publications, Volume 14, Issue 5, pp. 2647-54, Apr. 17, 2014

[6] J. Kim, M. Kim, M, Lee, K. Kim, S. Ji, Y. Kim, J. Park, **K. Na**, K. Bae, H. Kim, F. Bien, C. Lee, and J. Park, "Wearable Smart Sensor Systems Integrated on Soft Contact Lenses For Wireless Ocular Diagnostics," Nature Communications, Volume 8 Issue17, 2017

[7] N. Nguyen, S. K. Oruganti, **K. Na** and F. Bien, "An Adaptive Backward Control Battery Equalization System for Series Connected Lithium-lon Battery Packs", IEEE Transactions on Vehicular Technology (T-VT), Volume 63, Issue 8, pp.3651-3660, Oct., 2014

[8] S. Yoon, Y. Jang, C. Nam, S. Lee, J. Kwon, **K. Na**, K. Lee and B. Cho, "Sensitivity enhancement of a giant magnetoresistance alternating spin-valve sensor for high-field applications", Journal of Applied Physics 111 (7), 7, 2012

[9] **K. Na**, S. K. Oruganti and F. Bien, "An Improved Wireless Power Transfer System with Adaptive Technique for Implantable Biomedical Devices," IEEE MTT-S International Microwave Workshop Series on RF and Wireless Technologies for Biomedical and Healthcare Applications (IMWS-Bio 2013), Dec 9-11, 2013, Singapore

[10] H. Jang, **K. Na**, F. Bien, "A Stent based In-vivo Bio-sensing System for Glucose Monitoring," 2016 IEEE International Symposium on Radio-Frequency Integration Technology (RFIT2016) Howard International House, Taipei, Taiwan, August 24-26, 2016

[11] Fine pulse generator and method for generating fine pulse F. Bien, **K. Na**, Y. Choi, S.K. Oruganti US Patent 9,166,578, 2015